Field Behavior of Steel Threaded Micropiles under Axial Loads in Cohesive Soils

By

Zhengyang Guo

A thesis submitted in partial fulfillment of the requirements for the degree of

Master of Science

in

GEOTECHNICAL ENGINEERING

Department of Civil and Environmental Engineering

University of Alberta

Abstract

Steel threaded micropiles are a new deep foundation system recently introduced to the piling industry of North America. This pile consists of a steel threaded tubular shaft that is tapered at the lower segment. Steel threaded micropiles are quick to install, easy to dismantle, and have been increasingly used to support new and existing structures. Therefore, it is important to study the performance of steel threaded micropiles installed in different soil types subject to various loading conditions. Although conventional micropiles have been investigated in a limited number of studies, there is not any study of the axial performance of steel threaded micropiles.

Field tests of steel threaded full-scale micropiles with the diameter varying from 76 mm to 114 mm and length varying from 1.6 m to 3 m were carried out to investigate the axial bearing capacities, the load-transfer mechanism, the torque mechanism, and the axial cyclic response of the piles. Two cohesive soil sites were selected for the field tests: University of Alberta South Campus Site and Sherwood Park Site. Comprehensive site investigations including cone penetration tests (CPT), Shelby tube soil sampling, and laboratory tests were carried out for both sites.

At the South Campus site, forty load tests were performed on piles subject to static axial compressive and tensile loads. Four test piles were instrumented with several strain gauge stations. Results showed the piles behave as frictional piles and reached the limit state before the displacement exceeded 10% of the pile diameter. The adhesion coefficient of the top smooth shaft at limit state was less than 0.1. The failure mode along the cylindrical threaded shaft was confirmed to be cylindrical shearing along the edge of the threads; the threads increased the axial capacities of the segment. Axial capacities of

the threaded tapered segment were 43% on average greater than that of a cylindrical segment with the equivalent volume. Compressive capacities of all test piles were estimated based on preceding load-transfer mechanism and the results agreed reasonably well with the measured capacities. A theoretical torque model was proposed to estimate the end installation torques using the CPT-based remolded soil strength; the results matched the measured end torques very well.

At the Sherwood Park site, twenty-five axial monotonic load tests and three axial cyclic load tests were performed. Three tests were instrumented with five strain gauge stations to investigate the unit shaft resistance development during the monotonic and cyclic loading. Results showed that the piles behave as frictional piles and skin friction is mobilized when the displacement reaches 5% to 10% of the pile diameter during monotonic load tests. With the similar installation torques, the compressive capacity of all test piles is greater than tensile capacity by an average of 27%. When subject to vertical earthquake loading, the steel threaded micropiles underwent acceptably small cumulative displacements of less than 2 mm. The magnitude of the cumulative displacement decreased with the pile length and pile diameter. Cyclic loading redistributed the load transfer along different segments of the pile and the negative skin friction was developed along the smooth pile shaft when the pile underwent decreasing axial loading. No degradation of pile axial stiffness was observed for the three piles tested under the range of applied cyclic loading.

Acknowledgements

Firstly, I wish to express my appreciation and gratitude to my supervisor Dr. Lijun Deng, whose selfless time and care were sometimes all that kept me going. Dr. Deng has been incredibly patient with me throughout this entire process, his insight, guidance and financial support were essential in completing this research.

I also truly appreciate Natural Science and Engineering Research Council of Canada (NSERC) under the Collaborative R&D program (CRDPJ 469600-14) for providing funding for this project and Industrial Postgraduate Scholarship for myself. Gratitude is also extended to Krinner Canada Inc. for the financial and technical support. Special thanks go to Benoit Trudeau, Dennis Lechot and William Carney of Workonthat Structure Inc. for the assistance in performing the field tests, and to Harra Vardeleon and Chunhui Liu for helping with the laboratory tests.

Next, I would like to thank my friends and colleagues at the university, particularly Abel Sanchez Juncal, Keshab Sharma and Weidong Li, for their companionship during the first two terms of classes and for countless unbelievably insightful coffee breaks.

Finally, I would like to thank my loving family. To my parents back in China, thank you for constantly believing and investing in me. Seven years have passed since I left home to experience the world on my own, your unconditional love is what kept me going. And to my husband Tianzhen, this thesis would not be written were it not for your persistent nagging every time I dare binge-watch Netflix on Friday nights or sleep in on Sunday mornings. Thank you for constantly keeping the kitchen counters clean, for being so incredibly supportive and patient, and most importantly, for always being there for me.

Table of Contents

List of Figures

List of Tables

1 Introduction

This chapter includes the background of the micropiles, objectives of this research, and the thesis organization.

1.1 Background

Micropiles (also known as minipiles, pinpile, and needle piles) are small-diameter (less than 300 mm), bored and grouted non-displacement piles that are typically reinforced with steel cages. Micropiles were first proposed by Fernando Lizzi in the early 1950's and were used in Italy for underpinning historic buildings damaged during the World War II (Bruce 1988). Micropiles were introduced to North America in 1973 and grew rapidly since the mid-1980s (FHWA 2005). Since then, micropile technology has evolved and the application is no longer limited to underpinning existing structures. Engineering applications of micropiles expanded to the seismic retrofit, embankment reinforcement, slope stability, and landslide prevention. In some cases, where the access is restricted, having the ability to withstand relatively significant axial loads, micropiles may be considered a substitute for conventional driven piles.

The current practice in micropile construction includes three main steps: drilling, placing reinforcement and grouting. A borehole is drilled with or without a temporary casing to a targeted depth, and the drill bit is removed before the reinforcement is placed into the borehole. The grout could be placed by gravity or pressurized as the temporary casing is being retracted. Occasionally the casing can be left in place and serve as a steel shaft. Due to the installation method, micropiles are classified as non-displacement piles and the grout-ground bond governs the pile capacity.

Steel threaded micropiles are a deep foundation system that has been recently introduced to North America piling industry. Threaded micropiles consist of a steel tube with continuous spiral

threads welded on the lower half of the pile shaft and a close-end tapered pile tip. Depending on the application of the foundation system, pile caps of different size and geometry are welded on top of the pile shaft, making it easier to mount on the structure to be supported. Figure 1-1 shows a selection of threaded micropiles with different configurations.

Normally threaded micropiles are manufactured with a certain length, which ranges from 0.8 m to 5 m. Sometimes, it is desirable to install the piles at a specific deep soil layer to achieve optimum pile capacity. This could be achieved by installing extendable threaded micropiles, where extra threaded tubes can be bolted on top of the primary pile, forming a much longer pile. Therefore, there is no limitation on the pile length. The most commonly used threaded micropiles have diameters ranging from 66 mm to 140 mm.

This new foundation system is mainly used to support lightweight structures both axially and laterally. Figure 1-2 shows several engineering applications of steel threaded micropiles including mounting renewable energy system, fixing fences and gates, supporting wooden structures, and temporary event buildings.

Steel threaded micropiles are made of steel, with a galvanized coating to provide corrosion resistance. The installation method of steel threaded micropiles are different from conventional micropiles. Firstly, steel threaded micropiles are screwed into the ground by applying a torque to the pile head while a downward force is also applied to make the pile to advance downward. No pre-drilling is required prior to the pile installation unless in gravelly ground and no grouting is involved; therefore, the ground disturbance is minimum and the pile is immediately loadable after installation. Because no soil is removed prior to installation, this pile type can be classified as displacement pile, and the increase in lateral earth pressure caused by installation could potentially lead to a higher pile capacity than conventional micropiles. Secondly, concrete

grouting is not involved in construction of steel threaded micropiles, therefore no curing time is needed and the piles are immediately loadable after installation. The material and installation method are two key factors affecting the behavior of pile foundation. Given that the steel threaded piles are very different from conventional micropiles in these two aspects, the current design guideline of conventional micropiles may not be applicable on the new pile type.

The installation method of steel threaded piles is very similar to that of helical piles, which are also manufactured out of steel. Helical piles are deep foundation elements used to support axial compression, axial tension and lateral loadings (Bradka 1997), and normally consist of a central shaft, and one or multiple helical plates affixed to the shaft. Same as steel threaded micropiles, helical piles are also installed into the ground by applying a turning moment to the head of the central shaft while a downward force may also be applied so that the pile can advance downward in a "screwing" motion (Tappenden 2007). In the helical pile industry, the most commonly used design method is the torque factor method. First proposed by Hoyt and Clemence (1989), the torque factor is defined as the ratio between pile capacity and final installation torque. Due to the similarity in material and installation method, the installation torque is also measured and recorded for steel threaded micropiles. But the torque factor is site-specific and is largely depended on the pile configuration. Despite the similarity of steel threaded piles and helical piles, the design method for helical piles may not be applicable for the new pile type. Pile-specific load tests need to be carried out on the new pile type to evaluate the performance of the steel threaded micropiles.

1.2 Objectives

The objectives of this research are to:

- Investigate the load-transfer mechanisms along various segments of micropiles subject to axial compressive loadings and to develop a feasible method of predicting the axial capacities of the piles.

- Develop a theoretical torque model based on in-situ soil properties and pile characteristics and to verify the model using measured installation torques.

- Evaluate the response of steel threaded micropiles under cycles of one-way compressive loadings that simulate the vertical cyclic loadings induced by earthquake motions.

1.3 Testing Program

To fulfill the preceding objectives, a series of field load tests of full-scale steel threaded micropiles were carried out at two cohesive soil sites located in Alberta, Canada. At Site 1 located on the South Campus of the University of Alberta, six types of steel threaded micropiles were selected and tested under monotonic axial compression and tension loading. At Site 2 located in Sherwood Park, Alberta, the piles were tested under the monotonic axial loadings, and three piles were tested under axial cyclic loading. Comprehensive site investigations were conducted at both sites. Installation torque was measured for all tests to verify the value predicted by the theoretical torque model. Load versus displacement curves were obtained from each load test to evaluate the ultimate and limit state pile capacity of the piles. Selected piles were instrumented with strain gauges to measure the internal load distribution along the pile length and to characterize the load-transfer mechanism at the soil-pile interface. After the load-transfer mechanism was determined, a method of predicting pile capacity was proposed and verified by comparing the predicted values with measured capacity.

1.4   Thesis organization

This thesis is a paper-based thesis and consists of five chapters. Chapter 1 constitutes the introduction. Chapter 2 is the literature review on the previous studies on micropiles and helical piles subject to monotonic and cyclic loading patterns. Chapter 3 investigates the field performance of the steel threaded micropiles subject to monotonic axial loadings installed cohesive soils at the South Campus Farm Site. Chapter 4 investigates and compares the responses of steel threaded micropiles installed in cohesive soils at the Sherwood Park Site when subjected to axial cyclic and monotonic loadings. Chapter 5 summarizes the conclusions of this research program. Chapter 3 has been submitted to a peer-reviewed journal for possible publication and Chapter 4 is to be submitted. Although these two papers have multiple authors, the thesis author carried out the majority of the work, and therefore these papers are included in this thesis.

Appendix A is the LoggerNet codes for the data acquisition system. The testing apparatus was designed by the thesis author and the as-built structural design is attached in Appendix B.

(www.ground-screws.co.uk)

Figure 1-1: Schematic of steel threaded micropiles with various lengths and dimeters.

(http://www.krinner.co.uk/)

Figure 1-2: Selected applications of steel threaded micropiles.

2   Literature Review

This chapter summarizes the published literature in the development of micropile technique and the behavior of micropiles under axial monotonic and cyclic loadings.

2.1   Brief history of micropiles

Micropiles were first proposed by Fernando Lizzi in the early 1950's and were used in Italy for underpinning historic buildings damaged during World War II (Bruce 1988). Dr. Fernando Lizzi is commonly recognized as the inventor of micropiles in the form of the root pile or palo-radice. There has been a rapid growth in the specification and use of micropiles in the United States since the mid 1980's to early 1990's partly as a result of US Federal Highway Administration (FHWA) research efforts, trade association promotion efforts and the development of various publications offering standardized design and specification guidelines (FHWA 2005). Since then, the micropile technology has evolved and the application is no longer limited to underpinning existing structures. Engineering application of micropiles expanded to seismic retrofitting and reinforcing embankment, slope and landslide (Drbe and El Naggar 2015).

With the increasing demand of micropile in the foundation industry, many studies have been carried out to investigate the behavior of micropile subject to axial loading. However, because micropile is a general term for piles with small diameter, in current practice, micropiles vary in terms of geometry, installation method and material, and these factors have enormous impact on the micropile performance. When analyzing the behavior of micropiles, it is necessary to focus on the specific effect of each variables.

Bruce and Yeung (1984) stated that the geotechnical capacity of micropiles is dictated by the shear resistance at the grout / ground interface and settlements of 10% to 20% of the pile diameter is required to mobilize the pile capacity. Juran et al. (1999) and Cadden et al. (2004)

found the key contributor to micropile load transfer was the skin friction, and the toe bearing resistance of micropiles were negligible due to the small toe area. Han and Ye (2006) carried out a field study of single micropiles in soft clay under compression or tension and concluded that the ultimate compressive skin friction for micropiles was 0.9 to 1.2 times the undrained shear strength.

2.2 Monotonic loading

2.2.1 Load-transfer mechanism

Skin friction or adhesion resistance is established on the shaft-soil interface of the micropile. For piles in cohesive soil, there are two approach to calculate skin friction: total stress analysis and effective stress analysis. Tomlinson (1957) recommended an adhesion coefficient of 0.58 for driven piles in medium stiff clayey soils using a total stress approach. Adhesion coefficient α (when undrained shear strength of the soil is less than 100 kPa) can be calculated from:

$$\alpha = 0.21 + 0.26 p_a / s_u (\leq 1) \tag{2-1}$$

where p_a is the atmospheric pressure.

Randolph and Murphy (1985) suggested established an incremental method to estimate skin friction, where the adhesion coefficient is related to the strength ration s_u/σ'_v. The peak skin friction at any depth is estimated from:

$$\tau_s = [(s_u / \sigma'_v)_{nc}]^{0.5} s_u^{0.5} \sigma_v'^{0.5} \tag{2-2}$$

when the strength ratio is less or equal to unity, and

$$\tau_s = [(s_u / \sigma'_v)_{nc}]^{0.5} s_u^{0.75} \sigma_v'^{0.25} \tag{2-3}$$

when the strength ratio is greater than unity.

Current literature suggests that shaft roughness (smooth vs. threaded shaft, Cuthbertson-Black 2001) have significant impacts on the pile axial behavior. Cuthbertson-Black investigated the interaction between a flighted steel pipe pile and frozen sand and concluded that the rate of load transfer through the flighting section was higher than the rate of load transfer through the smooth shaft section. At the maximum applied load, even though the flighted section only made up approximately 50% of the pile length, it carried up to 75% of the applied load, while the smooth shaft only carried 18%. The flighted pile geometry is very similar to the steel threaded micropiles studied in this research program. Unfortunately, no conclusion could be determined as to whether the load transfer by the flighting was through adfreeze, bearing, or a combination of both.

The continuous flight of the steel threaded micropiles have a similar characteristic to helical piles with multiple helices. It has been established that helical piles with multiple helices have two possible failure mechanisms: individual bearing mode (IBM) and cylindrical shear mode (CSM) (Meyerhof and Adams 1968; Mooney et al. 1985; Narasimha Rao et al. 1991; Zhang 1999, Livneh and El Naggar 2008; Elsherbiny and El Naggar 2013).

Narasimha Rao (1991) tested model helical piles in soft and medium stiff clays prepared in a test tank and concluded that by keeping the ratio of the spacing of the helical plates to diameter of the helical platers between 1.0 and 1.5, optimum capacities of the piles could be obtained and the failure surface is very nearly cylindrical.

Livneh and El Naggar (2008) carried out full-scale load tests in different soils and numerical modeling on helical piles with three helical bearing plates with an *S/D* ratio equals to 3 (*S* is the spacing between helical plates and *D* is the diameter of the helical plates). It was found that the load transfer to the soil is predominantly through a cylindrical shear failure surface.

Elsherbiny and El Naggar (2013) investigated the compressive capacity of helical piles in sand and clay by means of field testing and numerical modeling. Piles tested in clay soils have two or three helices affixed to the cylindrical pile shaft. The S/D ratio ranged from 2 to 3. It was found that in cohesive soil, although the load-transfer mechanism is through individual bearing, numerical modeling results shows that a soil cylinder is starting to form between the helices near failure. Therefore, a cylindrical shear failure mechanism is appropriate for piles with helices embedded in cohesive soils.

The closed-end tapered segment of steel threaded micropile is similar to the configuration of a tapered pile. The axial behavior of tapered piles was characterized by a limited number of researchers.

Rybnikov (1990) conducted field tests on seven bored cast-in-place tapered piles with a taper angle of 1˚20', 2˚ and 2˚40' in sandy loam and sand. It was found that the specific pile capacity of a tapered pile was 20%-30% greater than that of a cylindrical pile having the same length, where the specific pile capacity is defined as the axial capacity per unit shaft volume. Additionally, because the pile capacity and material cost increase in direct proportion to the increase in taper angle, it was also concluded that within the investigated limits, the most rational pile type is a bored-cast-in-place pile with a taper angle of 2.5˚.

Kodikara and Moore (1993) developed a simplified theoretical model for piles with taper angles of 1° to 5° in cohesive soils. It was found that in contrast to cylindrical piles, the side resistance of tapered piles continues to increase with the axial deformation because of the additional radial expansion of the ground caused by the tapered pile wall. And it was concluded that the shaft resistance of tapered piles is substantially greater than that of cylindrical piles of equal shaft volume.

Wei and El Naggar (1998) carried out experimental study of axial behavior of model tapered piles installed in sand. The soil was contained in a steel soil chamber and pressurized using an air bladder to model the confining pressure. The results indicate a beneficial effect of pile taper in terms of an increase in the axial capacity and stiffness. Due to the taper, an increase in the shaft resistance can be expected because the sand adjacent to the pile was forced to expand radially and additional lateral pressures developed and caused an increase in the shear stress across the pile-soil surface.

El Naggar and Sakr (2000) investigated the performance of tapered piles in cohesionless soils under axial compressive loading using centrifuge model tests and proposed a simplified design approach for tapered piles. Three instrumented steel piles with different degrees of taper were tested in the sand chamber, and it was concluded that due to the taper, an increase in the shaft resistance could be expected because the sand adjacent to the pile was forced to expand radially, and additional lateral pressures developed and led to increases in the shear stresses across the pile–soil surface. However, the extent of the taper was most efficient in the upper length corresponding to 20 times the pile diameter, it was recommended that the taper be confined to the topmost part of longer piles.

2.2.2 Installation torque

The installation method of steel threaded micropile is similar to that of helical piles. The installation torque is of primary importance in the evaluation of axial capacities of helical piles in the design practice. Empirical torque–capacity correlation is being used for design purpose.

Hoyt and Clemence (1989) suggested a direct empirical relationship between installation torque and screw pile uplift capacity:

$$Q_u = K_t T \tag{2-4}$$

where K_t is the empirical torque factor with a unit of m^{-1}, Q_u is the uplift capacity and T is the average installation torque (kN*m).

Ghaly and Hanna (1991) developed a relationship between the measured uplift capacity of screw piles installed in sand and the final installation torque. The relationship is based on a theoretical analysis of the forces involved in resisting the insertion of the screw pile into the sand, thus determining the torque required for installation. A torque factor based on the pile geometry, the installation depth and the unit weight of the sand was introduced.

Sakr (2015) proposed a theoretical torque model to estimate the torsional resistance of cohesionless soils to the helical pile installation. He also listed the factors that affect the helical pile installation, including soil properties, fluctuation in groundwater levels, the shape of pile shaft, pile geometry, and method of helical pile installation. The proposed model for predicting torsional resistance was validated by total of 52 field installation reported in the literature. The results show that the proposed theoretical model can be used to reasonably estimate the torque required to install round-shaft piles in cohesionless soils.

2.3   Micropiles subject to axial cyclic loadings

There is very limited research on the performance of micropiles subject to axial cyclic loads. Many structures such as transmission towers, solar system panels, and offshore platform are supported on pile foundations or pile groups; they are often subjected to cyclic environmental loads such as wind, waves, and earthquakes in both the axial and lateral directions (El Naggar and Wei 2000). It is acknowledged that the response of micropiles to cyclic loads is complex (Chan and Hanna 1980) and hence the site-specific field tests may be necessary to investigation the soil-pile interaction during the cyclic loads.

Poulos and Sim (1990) conducted a theoretical analysis on five different "engineered" pile types. The program GAPCYC was used and the consideration of cyclic degradation was confined to skin friction. It was concluded that the cyclic performance of a pile may be improved by adjusting its diameter and/or stiffness. A pile taper could have a favorable effect on its cyclic performance as it reduced the stress concentration.

El Naggar and Wei (2000) investigated the effect of taper on the cyclic response of model tapered piles axially loaded in a pressurized steel sand chamber. Three instrumented steel model piles with different degrees of taper were installed in loose sand and subjected to two-way cyclic axial load tests. It was observed that the amplitude of the cyclic load had a significant effect on the performance of the piles. It was concluded that the pile stiffness increased with the number of load cycles, given that the load amplitude did not approach the uplift capacity of the pile. Additionally, the performance of tapered piles under cyclic load was found to be superior to that of straight-sided wall piles.

Cavey et al. (2000) studied the pressure-grouted micropiles in loose to medium dense sand in order to evaluate the load-carrying capacity of the piles under reversed-direction cyclic loading conditions. The results showed considerable reduction in capacity after only two cycles of loading as low as 60% of the ultimate capacity. This observation indicates that micropiles installed in cohesionless soil have a critical level of repeat loading that is well below the ultimate pile capacity under static conditions.

Abd Elziz and El Naggar (2012) carried out a field study of the behavior of single hollow core micropiles in stiff clay deposit. After 15 cycles with cyclic load amplitude of 33% of the micropile design load, the stiffness of most micropiles remained almost constant. However, the pile head movement increased after cyclic loading due to limited strain softening behavior of the

soil deposit. It was concluded that the micropile's performance in stiff clay is not sensitive to minor changes in cyclic load amplitudes, but sensitive to the magnitude and rate of the total applied load.

Drbe and El Naggar (2015) carried out full-scale load test to evaluate axial monotonic and cyclic compression behavior of hollow-bar micropiles and observed no change to a slight increase in the pile head stiffness after 15 axial load cycles of hollow core micropiles installed in cohesive soils.

3   Field behavior of steel threaded micropiles subject to axial loading in cohesive soils[1]

Abstract

Field tests of steel threaded full-scale micropiles with diameter varying from 76 mm to 114 mm and length varying from 1.6 m to 3 m were undertaken to investigate the axial bearing capacities, load-transfer mechanism, and the end installation torques of the piles in cohesive soils. Forty load tests were performed on piles subjected to static axial compressive and tensile loads. Four test piles were instrumented with several strain gauge stations. Results showed the piles behave as frictional piles and reached the limit state before the displacement exceeded 10% of the pile diameter. The adhesion coefficient of the top smooth shaft at limit state was less than 0.1. The failure mode along the cylindrical threaded shaft was confirmed to be cylindrical shearing along the edge of the threads; the threads increased the axial capacities of the segment. Axial capacities of the threaded tapered segment were 43% on average greater than that of a cylindrical segment with equivalent volume. Compressive capacities of all test piles were estimated and the results agreed reasonably well with the measured capacities. A theoretical torque model was proposed to estimate the end installation torques; the results matched the measured end torques very well.

3.1   Introduction

Micropiles are piles with small diameters, normally ranging between 100 mm and 300 mm. Micropiles were introduced to underpin historic buildings damaged during World War II in Italy (Bruce 1988). Applications of micropiles include supporting light axial and lateral structural loads, replacing or underpinning existing foundations, reinforcing embankment, slope and landslide, and seismic retrofitting. Current practice of micropile installation includes the following steps: drilling to a targeted depth, placing steel reinforcement, and placing or

---

[1] This chapter has been submitted to Canadian Geotechnical Journal for possible publication.

pressurizing the grout (FHWA 2005). Micropiles have advantages when there are difficult ground conditions such as limited access to construction sites due to natural or manmade obstruction. Another advantage is that the pile capacity is often attainable by full-scale loading tests due to the relatively small size of the pile (Coduto 2001).

Steel threaded micropiles, a new foundation type, have been recently introduced to the foundation construction industry of North America. This pile type consists of the smooth cylindrical segment on the top, threaded cylindrical segment in the middle, and threaded tapered segment at the bottom. Unlike conventional micropiles, this pile type is made of a steel tubular shaft with continuous spiral threads. This pile type is screwed into the ground, which minimizes the ground heave and fully displaces the soil to maximize the lateral earth pressure on the shaft.

Although the steel threaded micropile may potentially be useful in many applications, research on the axial behavior of this pile type is currently unavailable. The geotechnical design of this pile type largely depends on site-specific load tests, which are costly although attainable. There is no acceptable design guideline for this pile type or similar in the literature. Current literature suggests that pile shape (tapered vs. straight shaft, Wei and El Naggar 1998), shaft roughness (smooth vs. threaded shaft, Cuthbertson-Black 2001), and installation methods (drilled, driven, or screwed-in, Salgado 2008) have significant impacts on the pile axial behavior. Due to the unique characteristics, steel threaded micropiles may perform differently from conventional piles.

The closed-end tapered segment of steel threaded micropile is similar to the configuration of a tapered pile. The axial behavior of tapered piles was characterized by a limited number of researchers. Rybnikov (1990) conducted field tests of bored cast-in-place tapered piles in sandy

soil and found that the specific pile capacity of a tapered pile was 30% greater than that of a cylindrical pile, where the specific pile capacity is defined as the axial capacity per unit shaft volume. Kodikara and Moore (1993) developed a theoretical model for piles with taper angles of 1° to 5° in cohesive soils, and concluded that the shaft resistance of tapered piles is substantially greater than that of cylindrical piles of equal shaft volume. El Naggar and Sakr (2000) investigated the effects of taper on the axial compressive capacity and proposed an analytical approach for the design of tapered piles in sand. Despite these, however, there is a lack of field experimental research in the capacities of the threaded, tapered piles that are installed into cohesive soils by torsion.

Hence, the first objective of the present research is to investigate the load-transfer mechanisms along various segments of micropiles subject to axial compressive loadings and to develop a feasible method of predicting the axial capacities of the piles.

The installation method of steel threaded micropile is similar to that of helical piles. The installation torque is of primary importance in the evaluation of axial capacities of helical piles in the design practice. Sakr (2015) proposed a theoretical torque model to estimate the installation torque of round-shaft helical piles in cohesionless soils. Empirical torque–capacity correlation is being used for design purpose (e.g., Hoyt and Clemence 1989, CFEM 2006, Ghaly and Hanna 1991). Since helical piles and the steel threaded micropiles are both screwed into the ground, the installation torque may also be useful in predicting the axial capacities of micropiles and an understanding of the torsion resistance during micropile installation is vitally important. Therefore, the second objective is to develop a theoretical torque model based on in-situ soil properties and pile characteristics and to verify the model using measured installation torques.

To fulfill the preceding objectives, field load tests were carried out to characterize the performance of steel threaded micropiles under mainly axial compressive loads. Full-scale steel threaded micropiles of six sizes were tested at a cohesive soil site located in Edmonton, Canada. Site investigation consisting of cone penetration tests (CPT), Shelby tube sampling, and laboratory tests of intact soil samples was carried out to obtain the profiles of soil strength and physical properties. Each pile load test was repeated for at least three times to observe the consistence in the results. Axial loading, displacement, and the installation torque were recorded. Four research piles were instrumented with strain gauges at five stations and the results are presented in detail. Although axial tension tests were conducted, the present research will focus on the axial compression performance of piles based upon attained high-quality strain gauge records.

Based on the results of instrumented piles, the adhesion coefficient along the smooth segment was determined, the failure mechanisms of the threaded cylindrical shaft were characterized, and effects of the tapered tip on the axial capacities were quantified. The axial capacities at the limit state of all test piles were estimated and compared with the field-measured capacities. A theoretical torque model was proposed using the remolded soil strength based on the sleeve friction from CPT soundings; the model was validated by the measured end installation torques of all test piles.

3.2   Pile Description

Steel threaded micropiles (shown in Figure 3-1) in the present research consist of a hollow tube with continuous spiral threads welded on the lower shaft. This pile type is manufactured in different lengths and diameters, commonly used sizes range from 66 mm to 140 mm in diameter and 0.8 m to 5 m in length. This pile type is made of structural steel coated with galvanization

for corrosion resistance. This pile type is installed under torsion. Steel threaded micropiles may have several advantages over conventional micropiles. They are quick to install, easy to dismantle, reusable, and immediately loadable. No earth work is required prior to installation and the terrain remains undamaged after the piles have been removed. Because of the relatively small size and the installation method, the equipment required for installation is small compared to that for many other driven piles.

In present research, six types of steel threaded micropiles were tested under axial compression and tension. Test pile types varied in length (L), diameter (D), and the tip shape. The configuration of each pile type is summarized in Table 3-1 and shown in Figure 3-1. The spacing between threads (s_{th}) of all test piles is 50 mm. The thread width (w_{th}) and thickness (t_{th}) of all test piles are 12 mm and 2 mm, respectively. The thickness of the smooth shaft of all test piles is 3.6 mm.

Due to the tapered shape at the tip of the piles, the shaft diameter changes from top to tip of the pile. The diameters in Table 3-1 are referring to the outer shaft diameter of the smooth shaft. Table 1 also lists the average taper angle (θ) of the closed-end tapered segment, as shown in Figure 3-1. The pile shaft and threads are made of structural steel having a Young's modulus of 210 GPa and a yield strength of 248 MPa. The pile material conforms to German standards DIN EN 10219-1 (DIN 2006a) and DIN EN 10219-2 (DIN 2006b).

3.3 Site Investigation

A cohesive soil site is selected for the field tests of full-scale piles. Figure 3-2 shows the site located at the University of Alberta South Campus Farm, Edmonton, Canada. This site has been traditionally used for field tests of piles because it represents typical soil profiles observed in

greater Edmonton area. The soils at this site are mainly glaciolacustrine sediments as part of the

Glacial Lake Edmonton deposits formed about 8,000 year ago (Edwards 1993). Site investigation

includes CPT, Shelby tube borehole sampling beside CPT locations, and laboratory tests of intact

Shelby tube samples. Five CPTs were conducted on the test site as shown in Figure 3-3. Two

Shelby tube sampling boreholes (BH-3 and BH-4) of 5.1 cm diameter were drilled and soil

samples were obtained between 0.6 m and 2.7 m below ground surface.

CPT-0 through CPT-2 were conducted in the summer of 2014, and CPT-3 and CPT-4 in the

summer of 2016 when the field tests were carried out. Results of CPT-3 and CPT-4 dissipation

tests showed that the groundwater table was 5.3 m below ground surface, which is deeper than

the layer of interest. As shown in Figure 3-4, CPT results suggest that the site is composed of

approximately 1 m of silty organic clay underlain by a highly-plastic, medium-stiff clay layer of

4.5 m thickness.

The CPT results were used to estimate the undrained shear strength s_u of in-situ soil (as shown

in Figure 3-4c) using Equation 1 (Robertson and Cabal 2012):

$$s_u = \frac{q_t - \sigma_v}{N_{kt}} \tag{1}$$

where q_t is the corrected cone resistance, σ_v is the total vertical stress, and N_{kt} is the site-specific

cone factor. In the present research, N_{kt} of 14 is adopted based on previous experience with the

test site; this selection is confirmed by the laboratory strength tests. The s_u of intact Shelby tube

samples was measured using the unconfined compressive strength (UCS) tests and vane shear

tests. Lab-measured and estimated s_u are compared in Figure 3-4c. It appears that the lab-

measured s_u was fairly consistent with depth, with values ranging between 50 kPa and 110 kPa.

The s_u estimated from CPT results was overestimated in the upper, approximately 1 m thick soil; this discrepancy is likely due to the high cone resistance of the desiccated, organic crust. For soils below 1 m depth, s_u estimated from CPT was consistent with the lab-measured values. At 2.5 m, s_u converges to an average value of approximately 100 kPa. Because the sleeve resistance f_s is a reasonable estimation of the remolded undrained shear strength (Robertson and Cabal 2012), the sensitivity of the clay can be determined by the ratio of s_u to f_s. Results shows that the sensitivity ranges between 1 and 2, which implies that the clay has a low sensitivity (Skempton and Northey 1952) and which is compatible with the geological history of the site.

Figure 3-5 shows the moisture contents and Atterberg limits of samples at BH-3 and BH-4. The in-situ moisture content was close to or less than the plastic limit. Figure 3-6 shows that the soils are classified as CH. Void ratio of the intact soil samples ranged from 0.7 to 1.1 and the degree of saturation ranged from 80% to 95%.

3.4   Field Test Program

Carried out in the summer of 2016, the field test program consists of 40 axial compression and tension tests on 6 pile types. A minimum of three compression and three tension tests were carried out on each pile type. The piles P1, P3, P5, and P6 were instrumented with strain gauges measuring axial internal loadings. Field test program is described below.

3.4.1   Loading frame

A loading frame was developed following ASTM D1143 (ASTM 2007a) and D3689 (ASTM 2007b) with minor revisions. Figure 3-7 shows the reaction system consisting of a reaction beam, two reaction pile groups on the ends of the beam and connectors. The reaction beam is 4.2 m long and can accommodate two loading tests at one setup station, as shown in Figure 3-7a. For

each reaction pile group, there were four identical 2.1 m long screw piles with a diameter of 0.14 m; the pile group was vertically stiff enough such that negligible displacement was observed in the loading tests. The beam was connected to the reaction pile groups by steel plates and threaded steel bars. The load was supplied by a two-way hydraulic jack connected to the load cell and fixed on the reaction beam. The two-way hydraulic jack allowed the loading frame to serve for both compressive and tensile loading conditions using the same configuration. The spacing between any two piles (test or reaction piles) was at least five times the largest pile diameter according ASTM (2007a, b) to minimize the effects of adjacent piles. The loading frame was designed with an overall factor of safety of 2.5, if the allowable load of 400 kN is applied in the middle of the reaction beam.

3.4.2   Test procedure

Test procedure conformed to ASTM D1143 (ASTM 2007a) for axial compressive load test and ASTM D3689 (ASTM 2007b) for axial tensile load test. Procedure A: Quick Test in the ASTM standard was adopted. The capacity of the test pile was estimated based on the previous load tests of similar pile types. The load was applied at an increment of 5% of the anticipated pile capacity at plunging failure; if the pile did not fail at the anticipated capacity, the load was applied in the same increment until failure. During each load interval, the load was maintained constant for 5 min. After reaching failure, the pile was unloaded in four equal decrements. In the unloading stage, the load cell reading was normally very stable, so the time interval was revised from 5 min to 2 min. Pile setup time, which is the waiting period between the installation and the testing, was at least 48 hours for all piles.

3.4.3   Instrumentation

For all the tests, two linear potentiometers (LP) were used and the average of the two readings was taken as the displacement of the pile head. A cylindrical load cell with a capacity of 900 kN was selected; it can measure both tensile and compressive load. The installation torque was recorded at the last cycle of the torque head rotation using a pressure differential gauge integrated into the installation equipment. All instruments were calibrated prior to the field tests.

Strain gauges consisting of a full-bridge Wheatstone circuit were applied onto the external pile shaft to measure the internal axial loads. Five stations were located on the instrumented piles: one beneath the pile cap, one above the threads, one on the tip and the other two between the threads. Figure 3-1 shows the locations of the strain gauge stations and Table 3-1 lists the spacing between adjacent stations for all instrumented piles. Protective coatings were used to prevent the wires and gauges from being torn off during pile installation. Three layers of coating were applied: a layer of epoxy, a thin layer of rubber coating, and a thick layer of aluminum foil tape. The edge of the aluminum foil tape was sealed with rubber coating to prevent soil and water from entering the circuit. Lastly, the stations were wrapped by plastic tapes and a steel cover of 0.79 mm thickness is welded onto the pile to protect the gauges from physical damage. Despite the protective measures, several strain gauges were still damaged during the pile installation or uninstallation and therefore only the results of instrumented piles with complete strain gauge records are presented and discussed.

3.5   Results and Discussion

After tests, uninstalled piles were examined thoroughly to check the integrity of structural steel; no visible damage was observed on the pile shaft or threads. Figure 3-3 shows the layout of all test piles and the locations of instrumented piles P1 (P1-C4 and P1-C5), P3 (P3-C3), P5

(P5-C4 and P5-C5), and P6 (P6-C1), of which the results are presented and discussed. The pile

test ID (e.g. P1-C4) implies the pile type, test type (C for compression), and the repetition

number. Details of the field test program and results are presented in the test report (Guo et al.

2017).

3.5.1 Load vs. normalized displacement curve

Figure 3-8 shows the load vs. normalized displacement (w/D) curve for each pile type subject

to compression and tension. The pile capacity at limit state is defined as the maximum load a test

pile can sustain without reaching the plunging failure (Salgado 2008). From the loading curve, it

is observed that with the same diameter, longer piles (P1, P3, and P5) tend to have a greater pile

capacity than shorter piles (P2, P4, P6), and undergo less displacement to reach limit state. For

piles with same length but different diameters, larger piles tend to have a greater pile capacity

and greater stiffness than smaller piles. Most piles reached the limit state before w/D reaches 0.1;

this means that for the present micropiles installed in cohesive soils, the limit state capacity will

still govern the axial design, as would be anticipated for other piles in cohesive soils (Salgado

2008). For the six test piles, the limit state capacity ranges from 40 to 150 kN for compression

and 15 to 130 kN for tension. Generally, for the same pile type, the limit compressive capacity is

greater than the tensile capacity. A softening behaviour was observed after the piles reached the

limit state, when the resistance dropped with an increasing displacement. The softening

behaviour can be explained by the fact that the soil is lightly overconsolidated and that the post-

failure remolded s_u is less than the peak s_u. The CPT f_s and s_u profiles shown in Figure 3-4

confirm that the remolded s_u is less than the peak s_u.

3.5.2   Axial load distribution

For instrumented piles, the internal shaft load Q at a strain gauge station is calculated using Equation 2:

$$Q = \varepsilon EA \tag{2}$$

where ε is the measured strain gauge, E is the Young's modulus of the steel, and A is the cross-sectional area at the gauge station. In the tapered segment, A is revised to account for the change in wall thickness.

Figure 3-9 shows the load distribution of piles P1 and P5 at different stages of axial loading, while the last curve represents the load distribution at the limit state. The load distribution curves show that the smooth shaft resistance was almost negligible and the majority of axial load was carried by the threaded segment. The internal force is close to zero at the pile tip, which implies that the steel threaded micropiles behave as a friction pile. Coduto (2001) also suggested that for micropiles, due to the small diameter, the toe bearing capacity is normally neglected.

These instrumented piles are divided into three segments: smooth segment (between SG-1 and SG-2), straight threaded segment (between SG-2 and SG-4), and tapered threaded segment (between SG-4 and SG-5). Pile P1 has a unique shape where the diameter of the shaft changes twice along the length; strain gauges were only installed at the top and bottom of the first tapered segment, as a result the load transfer within the second tapered segment was not captured. For P1, the smooth segment is between SG-1 and SG-2, the straight threaded segment is between SG-2 and SG-3, and the tapered segment is between SG-3 and SG-4; the purpose of SG-5 was to measure the end bearing at the pile tip. In order to understand the load transferred to the soil at various segments at the limit state, the unit shaft resistance, q_{sL}, is calculated using Equation 3:

$$q_{sL_{ij}} = \frac{Q_{Li} - Q_{Lj}}{S_{ij}} \tag{3}$$

where q_{sLij} is the unit shaft resistance between Station i and Station j, Q_{Li} is the measured internal load at the limit state at Station i, and S_{ij} is the surface area of the shaft segment between Station i and Station j. Note that for threaded segments, the thread width was accounted for when calculating the surface area of the pile.

Figure 3-9 shows the calculated q_{sL} distribution of selected piles. It is observed that q_{sL} is the least along the smooth segment, increased at the threaded shaft and increased in the tapered shaft. Figure 3-9 suggests that the threads have a positive contribution to shaft resistance. In the tapered segments, unit shaft resistance is much greater than that of the straight threaded segment with the same diameter, which is apparently due to the tapered shape. Load-transfer mechanisms along each segment is quantified in detail in subsequent subsections.

3.5.3 Load transferred to smooth shaft

Load transferred to the smooth segment, Q_{sm}, can be calculated using Equation 4:

$$Q_{sm} = \alpha s_u \pi D L_{sm} \tag{4}$$

where α is the adhesion coefficient between soil and smooth shaft, L_{sm} is the length of the smooth segment. The term $\pi D L_{sm}$ represents the contact area between the smooth segment and surrounding soil.

To determine α at the limit state, measured q_{sL} for three compression tests of piles with a diameter of 76 mm was compared with the average s_u over the span of smooth segment, as shown in Figure 3-10. A linear trend line shows a slope of 0.0926, which equals α at the limit

state. This α is substantially less than the adhesion coefficients suggested in literature: Randolph and Murphy (1985) suggested a lowest α of 0.73 or driven piles in clay having a strength ratio (s_u/σ_v') greater than 1, and Tomlinson (1957) recommended an adhesion coefficient of 0.58 for driven piles in medium stiff clayey soils. Due to the torsional installation and the fact that the diameter of smooth segment is less than the external diameter (D plus $2w_{th}$) of threaded segment, the soil surrounding the smooth shaft might have been expanded and disturbed during the installation, leaving an annular cavity between the pile and soil, thus causing a very small α value. This annular cavity was often visible after pile installation. Because the soil and pile were not in a firm contact, adhesion along the smooth shaft was not sufficiently mobilized. In conclusion, the smooth shaft is not a key contributor to the pile capacity of micropiles in cohesive soils.

3.5.4 Load transferred to threaded shaft

In order to predict the limit shaft resistance of the threaded segment, the soil failure mode shall be determined. At the limit state, it is hypothesized that two failure modes may be applicable to the straight threaded shaft. Figure 3-11a and b show the possible cylindrical shear mode (CSM) and individual bearing mode (IBM) for soil failure. Because the pile load test is in accordance with ASTM D1143 (ASTM 2007a) Quick Test, there is not enough time for excess pore pressure dissipation when the failure occurs; therefore, the soil is considered in undrained condition and the soil resistance is calculated using s_u.

For the CSM shown in Figure 3-11a, the soil between the threads and pile is assumed to behave as one complete unit, and the shear plane is a cylindrical surface on the outer edge of the threads. When the pile is displaced, the resistance arises from the s_u of the shaft-soil cylinder.

The limit load transferred to the straight threaded segment under the CSM hypothesis, Q_{th}, was estimated using Equation 5:

$$Q_{th} = (s_u)_{avg} \pi (D + 2w_{th}) L_{th} \tag{5}$$

where $(s_u)_{avg}$ is the CPT-based average undrained shear strength along the threaded segment, D is the smooth shaft diameter, w_{th} is the thread width (11 mm), and L_{th} is the length of the threaded segment. The term $\pi(D + 2w_{th})L_{th}$ is essentially the contact area between the soil and pile shaft that considers the thread width. For piles P3, P5 and P6, as shown in Figure 3-1 and Table 3-1, L_{th} equals $(L_2 + L_3)$, and for P1, L_{th} equals L_2.

For the IBM shown in Figure 3-11b, each thread is considered an individual bearing plate, and the smooth shaft between two threads provides upward shaft resistance. The limit load transferred to the threaded segment Q_{th} under the IBM hypothesis was estimated using Equation 6a:

$$Q_{th} = \sum_{i=1}^{m} \left(N_t (s_u)_i + (\sigma_v)_i \right) \pi (D + w_{th}) w_{th} + \alpha (s_u)_{avg} \pi D L_{th} \tag{6a}$$

where m is the number of threads within the threaded segment, N_t is the bearing capacity coefficient that equals 9 in present study (CFEM 2006, Salgado 2008), s_u and σ_v are the CPT-based undrained shear strength and total stress at the depth of individual threads. Equation 6a considers the annular threads as individual deeply-embedded strip footings. The term $\pi(D + w_{th})w_{th}$ is the projected area of each thread and the term $\alpha (s_u)_{avg} \pi D L_{th}$ is the adhesion around the pile shaft. Because the adhesion coefficient is very small as observed in preceding

subsection, the contribution of the shaft resistance is insignificant. Hence, Equation 6a could be expressed as:

$$Q_{th} = \sum_{i=1}^{m} \left(N_t \left(s_u \right)_i + \left(\sigma_v \right)_i \right) \pi (D + w_{th}) w_{th}, \text{ neglects shaft resistance} \tag{6b}$$

Figure 3-12 shows the estimated Q_{th} based on two possible failure modes vs. the measured load transferred to threaded shaft for six instrumented piles in compression tests, following Equations 5 and 6b respectively. It appears that the CSM assumption, although not perfect, better predicts the axial load in the threaded shaft than the IBM assumption. The IBM assumption overestimates Q_{th} by about 200%, even though the pile shaft adhesion has been neglected. For all test piles, the ratio of thread spacing s_{th} to thread width w_{th} is 50/12 or 4.2. The literature on helical piles (Narasimha Rao et al. 1991, Elsherbiny and El Naggar 2013) suggested that the ratio has a significant effect on the failure mode; smaller ratio leads to CSM for helical piles. Hence it is concluded that the ratio of 4.2 of present test piles is small enough to mobilize the CSM in present medium-stiff cohesive soils. In conclusion, the failure mechanism along the threaded segment is cylindrical shearing of the surrounding soil, as suggested in Figure 3-11a. The presence of threads pushes the shear failure surface outward to the edge of the threads, increases the "adhesion coefficient" to 1, and thereby enhances the pile capacity.

3.5.5 Load transferred to tapered threaded shaft

When studying the compressive capacities of tapered piles, one approach is to normalize the pile capacity by the pile shaft volume (termed the specific bearing capacity). Rybnikov (1990) found that the specific bearing capacity of a tapered pile in sand was 1.3 times that of a cylindrical pile. Wei and El Naggar (1998) showed that under different confining stresses, the specific shaft resistance of a tapered pile in sand was 1.13 to 1.65 times that of a cylindrical pile.

The present study investigates the effects of the tapered shape on pile capacities. We begin with comparing the measured limit axial load of the tapered shafts with the estimated axial load of a cylindrical shaft of equal volume. If we assume an equivalent, cylindrical shaft that has the same shaft volume as the tapered shaft, then we can adopt the CSM for the *equivalent shaft* based on the preceding observation on cylindrical threaded shafts. The limit load transferred to the *equivalent shaft* (Q_{tp_eq}) can be calculated using Equation 7:

$$Q_{tp\_eq} = \left(s_u\right)_{avg} \pi (D_{avg} + 2w_{th}) L_{tp} \tag{7}$$

where D_{avg} is the average shaft diameter of the tapered shaft, L_{tp} is the total length of the tapered segment, and $(s_u)_{avg}$ is the average s_u of the soil surrounding the tapered segment obtained from CPT strength profiles. The term $(D_{avg} + 2w_{th})\pi L_{tp}$ is essentially the slip surface area of the equivalent shaft. For piles P5 and P6, L_{tp} equals L_4, and for P1, L_{tp} equals L_3. Refer to Figure 3-1 and Table 3-1 for pile dimensions.

Figure 3-13 shows the estimated Q_{tp_eq} versus the measured Q_{tp} for four compression tests of two instrumented piles for which strain gauge records were attained at the segment. From the limited number of available data points, it appears that the measure Q_{tp} is greater than the Q_{tp_eq} by a factor of 10% to 80%. A linear trend line is plotted to show an empirical relationship between measured and estimated values. It is observed that for the four tests the actual load transferred to the tapered segment is greater than Q_{tp_eq} by 43% on average. The average taper angle of 5.2° and 5.5° was fairly large and thus may have increased the axial capacities significantly. As discussed in preceding research (e.g., Wei and El Naggar 1998), the reason for the capacity enhancement is that additional lateral pressure from the soil was induced and

resulted in an increase in shear stresses across the surface of tapered segment when the taper expands the adjacent soils.

3.5.6 Test pile axial capacities: measured vs. estimated

Now that the failure mechanisms of each segment have been preliminarily established from instrumented piles, the pile capacity of non-instrumented piles at the limit state, Q_L, can be estimated using Equation 8 in order to verify the preceding assumptions:

$$Q_L = Q_{sm} + Q_{th} + 1.43\left(Q_{tp\_eq}\right) \tag{8}$$

where Q_{sm}, Q_{th}, and Q_{tp_eq} are obtained from Equations 4, 5, and 7, respectively. For Equation 4, adhesion coefficient α equals 0.09 for the soil-pile interface as previously discussed. The coefficient of 1.43 in the Q_{tp_eq} term is empirically obtained from Figure 3-13. Average s_u along each segment was taken from the CPT strength profiles.

Figure 3-14a shows the estimated and measured limit capacities for all pile types. To account for the site heterogeneity when estimating Q_{Le}, we considered all of the CPT strength profiles as shown in Figure 3-4 and then obtained the maximum, minimum, and average values. Q_{Le} is shown in Figure 3-14a as error bars. It is seen that the majority of the measured capacities fall within or close to the estimated range except for two data points from P5. From Figure 3-14a, it is observed that the longer the pile, the wider the range of estimated pile capacity. For instance, the minimum Q_{Le} for P1 is about 80 kN while the maximum is about 150 kN; this is because the pile length, especially threaded length, plays a central role in contributing to the shaft resistance. The effect of heterogeneity of the soil on the pile pile capacity is amplified by the threaded length.

Figure 3-14b shows the average Q_{Le} versus the average Q_{Lm} for all six piles and the linear-fit trend line. It is observed that the average Q_{Le} is about 12% less than the average Q_{Lm}. The reason for underestimation could be due to underestimated $\square$, Q_{tp_eq}, or s_u because of the limited number of CPT soundings. Given the complexity of field tests and the heterogeneity of soils, however, a discrepancy of 12% on average is considered acceptable when estimating the pile axial capacities. As noted in Randolph (2003), "we may never be able to estimate the axial capacity in many soil types more accurately than about ±30%." Hence, it is reasonable to conclude that Q_{Le} based on Equation 8 is a good approximation to the measured Q_{Lm}, and the failure mechanisms proposed in preceding subsections are valid.

3.5.7 End installation torque: measured vs. estimated

End installation torque was recorded at the last cycle of rotation during the installation process. At the last cycle of rotation, the pile does not advance downward but rather rotates in-place. At this moment, the soil surrounding the shaft has experienced large shear strain and is at the remolded state. Although the soil is being sheared in the horizontal tangential direction, the soil resistance to pile rotation is considered similar to the sleeve friction recorded in the CPT soundings because the glaciolacustrine soil at this site is fairly isotropic. Therefore, a theoretical torque model based on CPT sleeve frictions is proposed and examined using the measured end torques.

Figure 3-11c illustrates the proposed torque model, where the applied torque is counterbalanced by the torque produced by sleeve friction f_s acting on the pile shaft and the threads. The end installation torque, T, is estimated using Equation (9):

$$T = 2\sum_{i=1}^{m}\left((f_s)_i \, \pi \frac{(D_i + w_{th})^2}{2} w_{th}\right) + f_s(L - L_1)\pi\frac{D^2}{2} \tag{9}$$

where f_s is the sleeve friction measured from CPT, D is the diameter of smooth shaft, L is total length of pile, L_1 is the length of smooth shaft, m is the total number of threads, D_i is the smooth shaft diameter at each thread location. The first term of Equation 9 is the torque produced by the shear stress flow on the top and bottom surfaces of each thread and the second term by the shear stress flow around the smooth shaft between threads. Because the upper smooth shaft of the pile have shown not be in a firm contact with the soil and have a very low adhesion coefficient, the torque from the smooth shaft adhesion is neglected in Equation 9.

To account for the effect of the site heterogeneity on installation torques, f_s from all five CPT soundings were used when estimating the end torques using Equation 9. Figure 3-15a shows the average, maximum, and minimum estimated torques T_e for each pile type and six measured torques T_m (from both compression and tension tests) for each pile. The effect of site heterogeneity is implied in Figure 3-15a as the maximum and minimum error bars. It is seen that the majority of measured T_m fall within or close to the estimated ranges, despite a few outliers in the pile P2. The estimated and measured torques are averaged and compared as shown in Figure 3-15b. It appears that the average T_e shows a good linear correlation with the average T_m. The trend line shows that the average T_e is only 2% lower than average T_m. The results shown in Figure 3-15b validates the proposed torque model based on the CPT f_s profiles.

The significance of the torque model is that it correlates the soil strength parameter f_s to the installation torques. Once the installation torque is obtained, one can back-calculate f_s from Equation 9 and therefore estimate, with the proper soil sensitivity, the undrained shear strength at the pile location; finally, the limit pile capacity can be predicted.

3.6   Conclusions

Full-scale pile load tests were conducted on six steel threaded micropiles at a cohesive soil site. The micropiles consist of hollow steel shaft with threads welded onto the lower segment and a tapered pile tip. The diameter of test piles ranges from 76 mm to 114 mm, and the length ranges from 1.6 m to 3 m. Comprehensive site investigation was carried out and selected piles were instrumented with strain gauges. Following conclusions may be drawn:

1. In similar soil conditions, the limit state pile capacity of steel threaded micropiles under axial compression is greater than tension. Pile length, especially threaded length, has a more significant impact on pile capacity of pile than pile diameter. Given the same length, pile with a greater diameter tends to have a greater axial capacity, and has a stiffer behaviour. Given the same diameter, longer piles tend to have a greater axial capacity and a greater stiffness.

2. This pile type behaves as friction piles. End bearing is negligible. The majority of the limit load was carried by the threaded segment. The adhesion coefficient between smooth shaft and soil is lower than 0.1 on average because the torsional installation process expands the soils and created annular gaps between pile shaft and surface soils.

3. Soils around the straight threaded segment fail in the cylindrical shear mode at the limit state. The ratio of thread spacing to thread width is 4.2 for all test piles. The presence of threads pushes the shear failure plane outward to the edge of the threads and thereby substantially increases the limit capacity of the threaded segment. The estimated limit capacities of the threaded segment based on the CSM assumption well predicted the measured capacities of instrumented piles.

4. Taper shape increases the shaft resistance. For the instrumented test piles with 5.2° and 5.5° taper angle at the tip, the limit shaft resistance of the tapered segment, is 43% on average greater than that of a cylindrical, equivalent straight shaft with the same shaft volume.

5. Limit capacities of all test piles under compression were estimated using proposed adhesion coefficient, failure mechanism, and empirical relationship between tapered segment pile capacity and straight segment pile capacity. The estimated limit capacities of piles were 12% on average less than the measured capacities. Given the complexity of field tests and soil heterogeneity, the discrepancy may be considered acceptable.

6. A theoretical torque model was proposed to estimate the end installation torque at the last cycle of rotation. The torque model considers the torque induced by the remolded shear strength acting on the shaft and the threads below the smooth segment. The torque model adopts the CPT-based sleeve friction and accounts for the site heterogeneity. The estimated torques of all test piles were 2% on average less than the measured torques, which confirms the validity of the proposed torque model.

Table 3-1. Dimension of steel threaded micropiles used for field tests.

Pile ID	D (mm)	L (mm)	L_1 (mm)	L_2 (mm)	L_3 (mm)	L_4 (mm)	θ (°)
P1	114	3000	762	1148	229	612	5.5
P2	114	1600	N.A.	N.A.	N.A.	N.A.	5.5
P3	89	3000	660	890	1030	254	5.5
P4	89	1600	N.A.	N.A.	N.A.	N.A.	5.5
P5	76	3000	1753	457	483	254	5.2
P6	76	1600	520	375	318	210	5.2

Note: Symbol definitions are labelled in Figure 3-1. The spacing between threads (s_{th}) of all test piles is 50 mm. The thread width (w_{th}) and thickness (t_{th}) of all test piles are 12 mm and 2 mm, respectively. The thickness of the smooth shaft of all test piles is 3.6 mm.
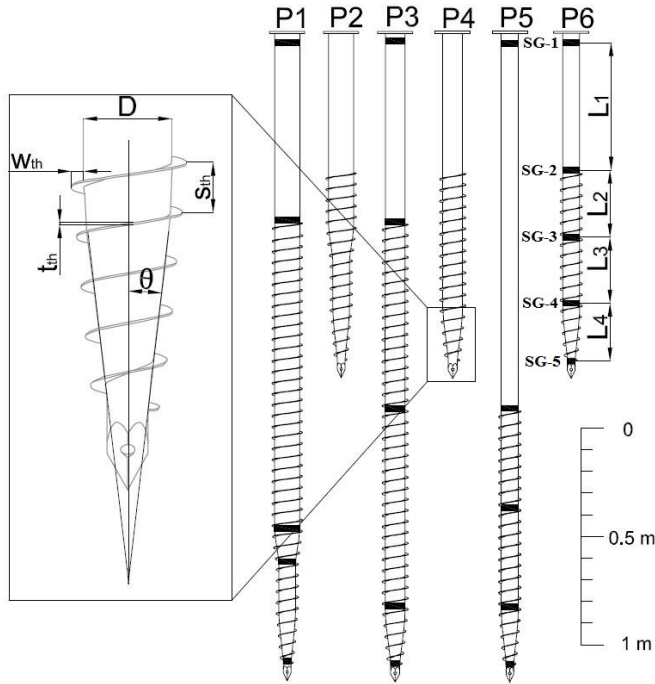
Figure 3-1: Schematic of test piles. Black strips on the shaft denote the locations of full-bridge strain gauge stations.

Figure 3-2: Map of test site located in Edmonton, Canada. Global coordinate of test site: N 53.498394, W 113.532756.
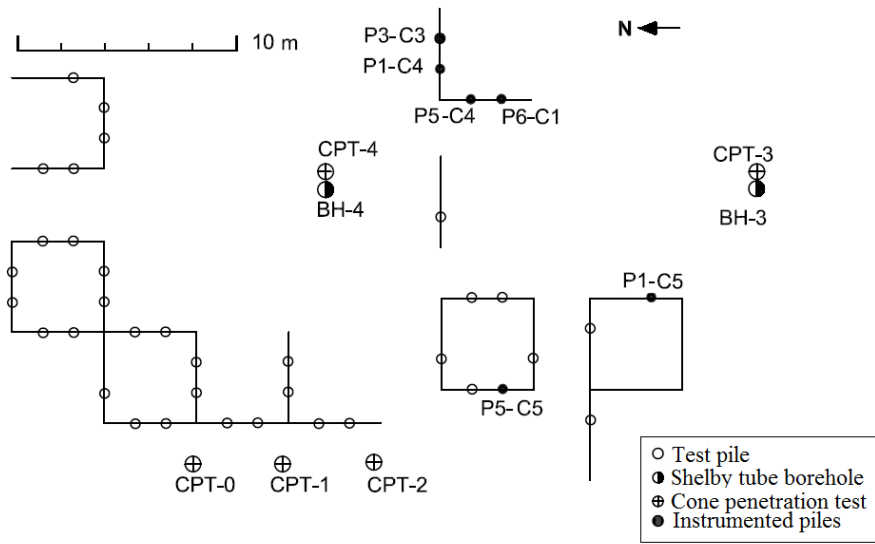
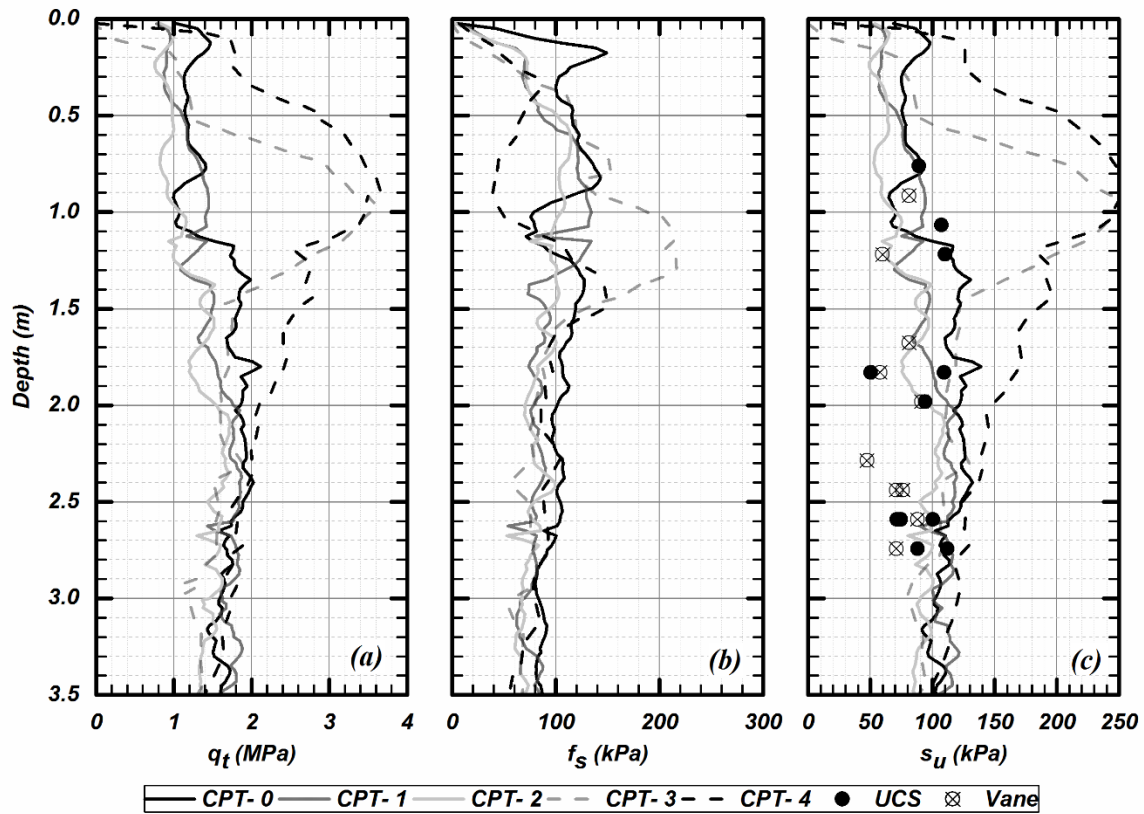Figure 3-3: Layout of CPT, Shelby tube boreholes (BH), and test piles.

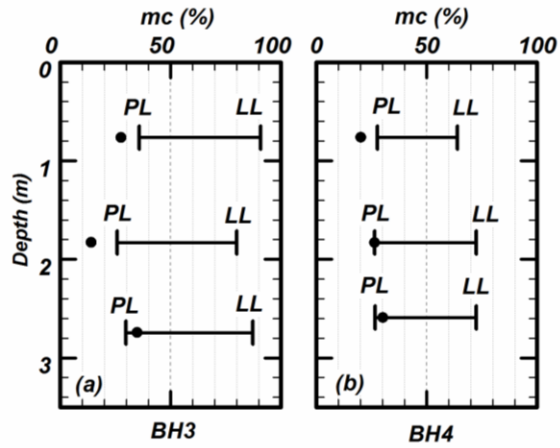Figure 3-4: CPT test results and undrained shear strength measured in laboratory.

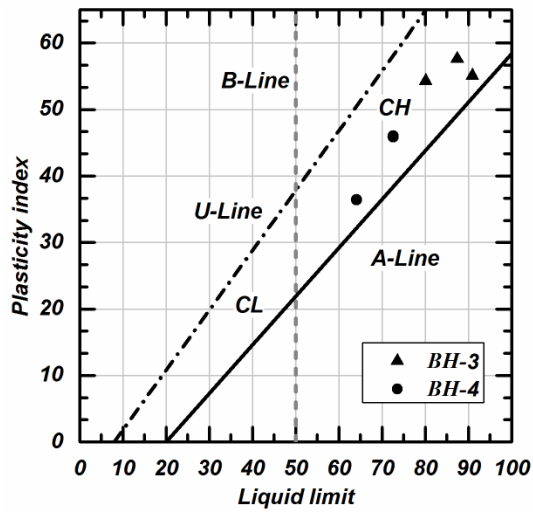Figure 3-5: Atterberg limit and natural moisture content (mc) of intact soil samples: (a) BH3 (b) BH4.

Figure 3-6: Plasticity chart for undisturbed soil samples from BH-3 and BH-4.
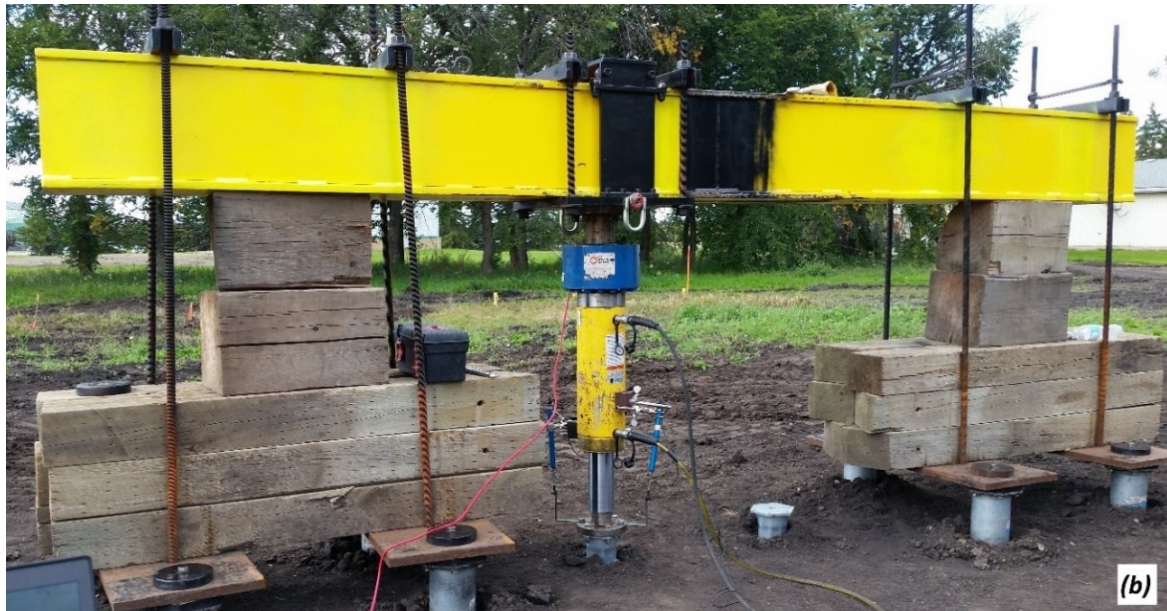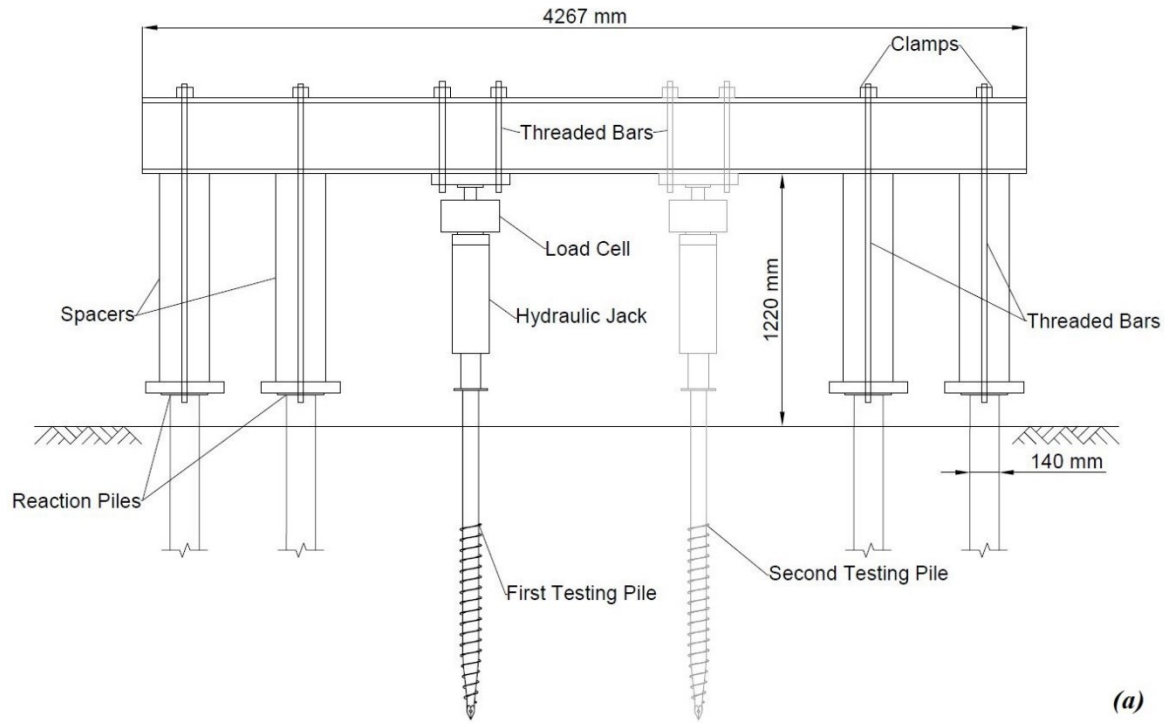
Figure 3-7: (a) Schematic and (b) photo of the load test apparatus.
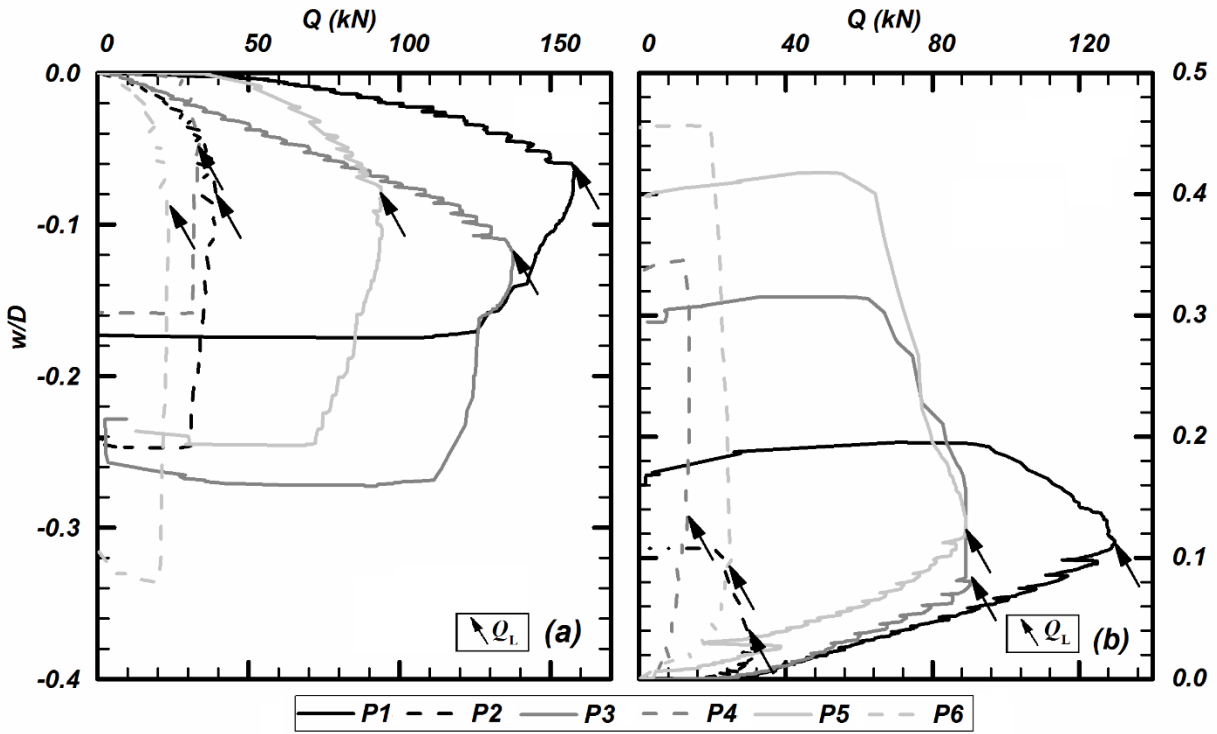
Figure 3-8: Selected axial load (Q) versus normalized axial displacement (w/D) curves for: (a) compression tests and (b) tension tests. D: diameter of pile shaft.
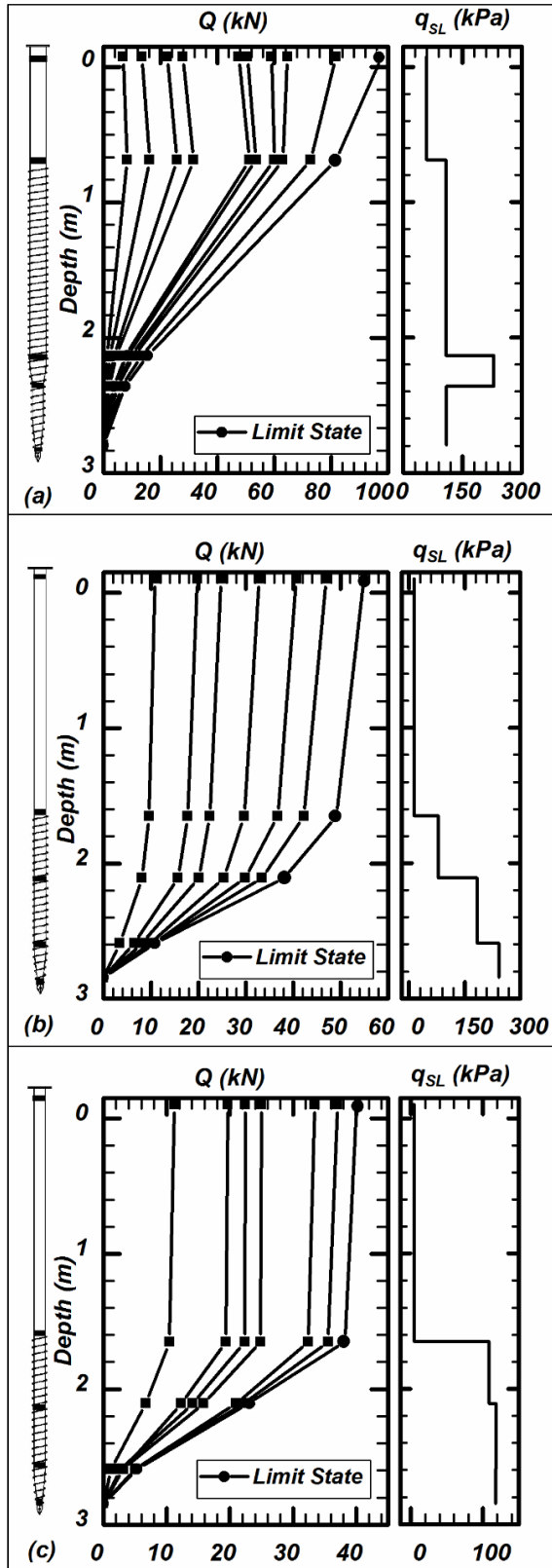
Figure 3-9: Axial loads transferred to pile shaft and unit shaft resistance at limit state (q_{sL}) for tests: (a) P1-C5, (b) P5-C4, and (c) P5-C5.
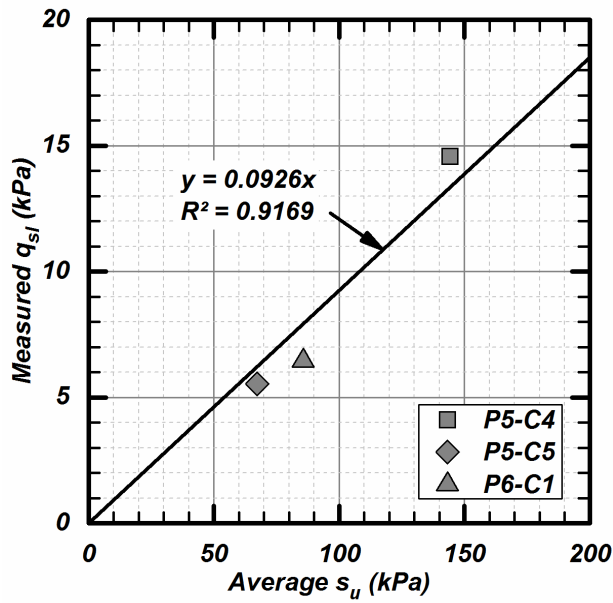
Figure 3-10: Measured q_{sL} vs. average s_u of the smooth shaft segment of selected instrumented piles. The shaft diameter of the piles P5 and P6 is 76 mm.
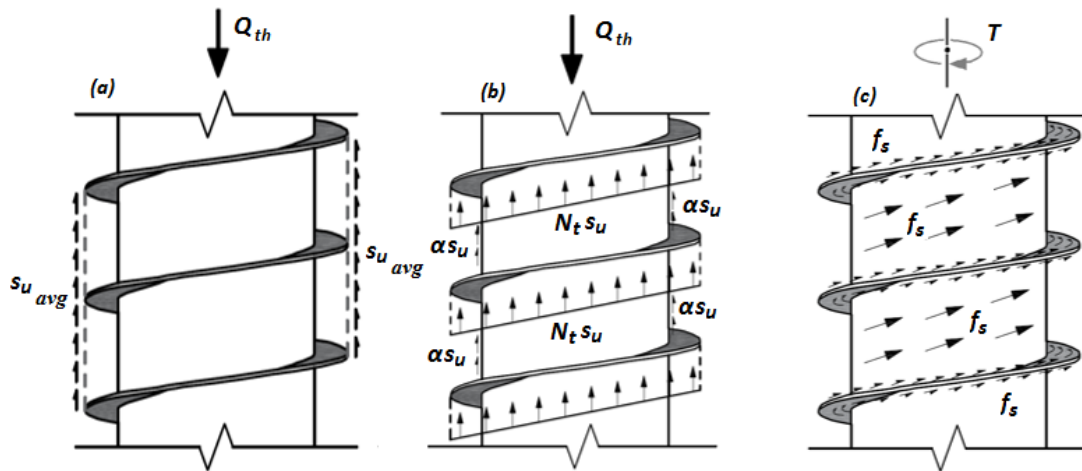
Figure 3-11: Hypothesized theoretical modes of axial failure in the threaded segment: (a) cylindrical shear mode (CSM) along the edge of threads, and (b) individual bearing mode (IBM) under each thread; and (c) proposed theoretical torque model, in which the applied torque is counterbalanced by the shear resistance from the threads and the shaft.
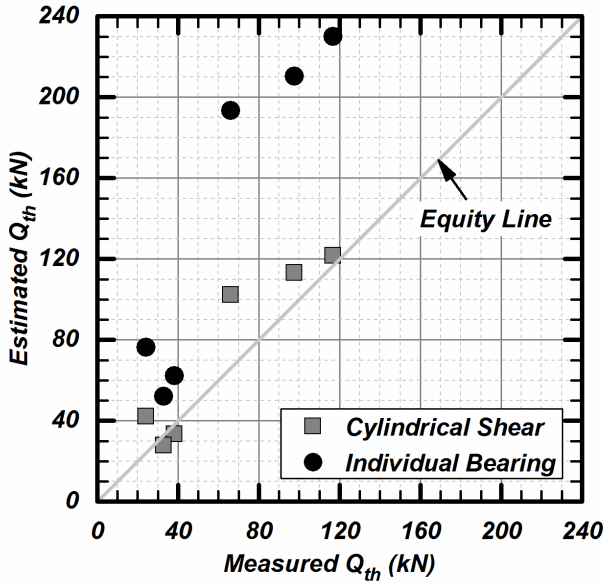
Figure 3-12: Estimated limit capacity Q_{th} vs. measured Q_{th} in the threaded shaft of selected instrumented piles. The estimations are based on the CSM and IBM hypotheses.
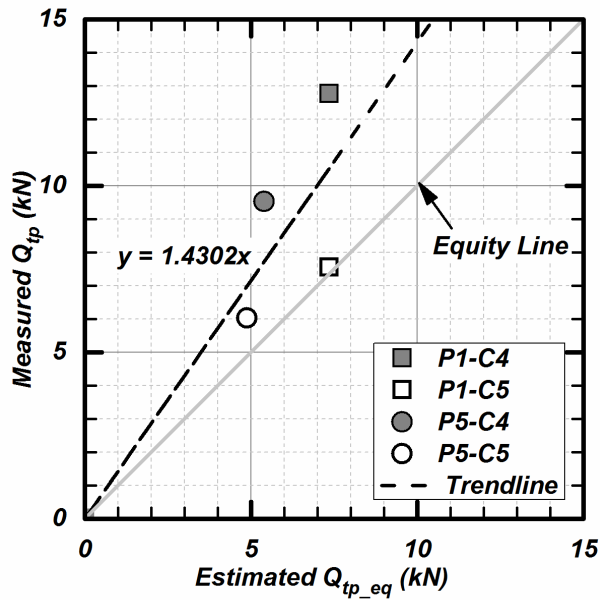
Figure 3-13: Measured limit capacity Q_{tp} vs. estimated Q_{tp_eq} of the threaded tapered segment of selected instrumented piles.
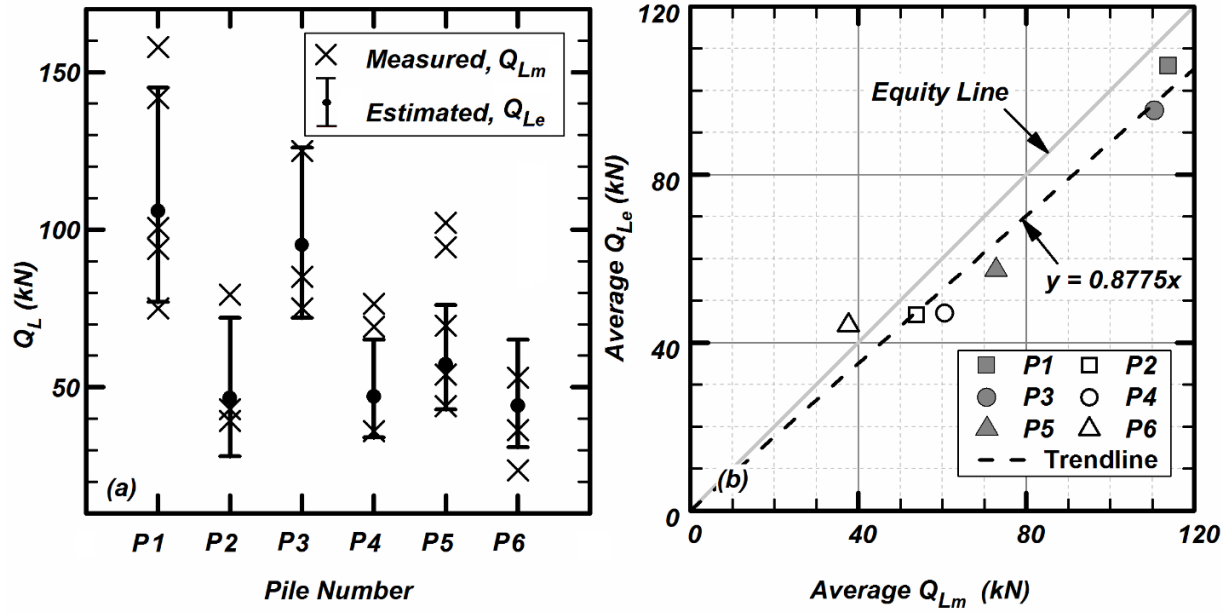
Figure 3-14: Limit capacities of all test piles: (a) estimated Q_{Le} of P1 through P6 vs. the measured Q_{Lm}, and (b) average estimated Q_{Le} vs. average measured Q_{Lm}. The estimated Q_{Le} is the sum of the limit capacities of the smooth segment, threaded segment, and the tapered threaded segment. The error bars in (a) show the minimum and maximum Q_{Le} due to the site heterogeneity as shown in the CPT s_u profiles.
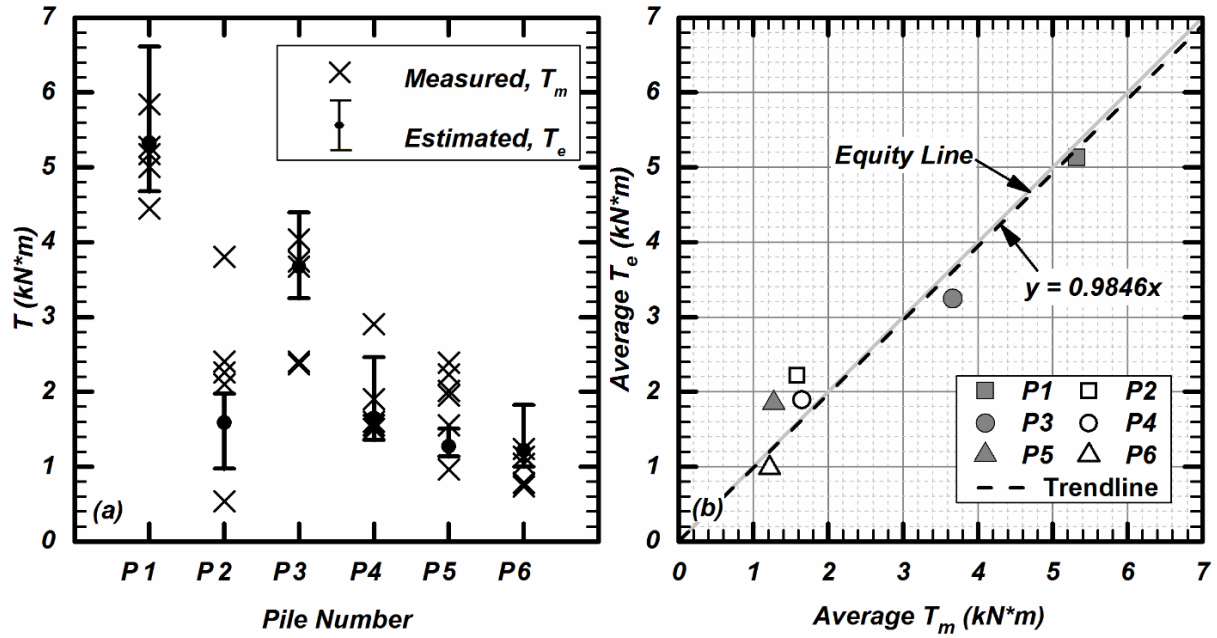
Figure 3-15: End installation torque T of all test piles: (a) estimated torques T_e of P1 through P6 vs. the measured torques T_m, and (b) average T_e vs. average T_m. The error bars in (a) show the minimum and maximum T_e due to the site heterogeneity shown in the CPT f_s profiles.

4 Field behavior of steel threaded micropiles subject to axial cyclic and monotonic loadings

Abstract

The steel threaded micropile is a new type of pile foundations recently introduced to the piling industry of North America. The pile type is used increasingly to support new and existing structures. However, there is not any research on the performance of the piles subjected to monotonic loading or axial cyclic loading due to the vertical ground vibration. In the present research, full-scale field tests of steel threaded micropiles were carried out at a test site located in Sherwood Park, Alberta. Selected test piles have a diameter varying from 76 mm to 114 mm and a length varying from 1.6 m to 3 m, and spiral threads welded on the lower half of the steel tube. Comprehensive site investigation revealed that the soil at the test site was medium to stiff, low plasticity clay. Twenty-five axial monotonic load tests and three axial cyclic load tests were performed on six pile types. Three tests were instrumented with five strain gauge stations to investigate the unit shaft resistance development during monotonic and cyclic loading. Results showed that the piles behave as frictional piles and the skin friction is mobilized when the displacement reaches 5% to 10% of the pile diameter during monotonic load test. With similar installation torques, compressive capacity for all test piles is greater than tensile capacity by an average of 27%. When subject to vertical earthquake loading, the steel threaded micropiles underwent small cumulative displacements and the magnitude of the displacement decreased with the pile length and pile diameter. Cyclic loading redistributed the load transfer along different segments of the pile and negative skin friction was developed along the smooth pile

shaft when the pile underwent decreasing axial loading during the cyclic loading cycles. Axial stiffnesses of cyclic and monotonic tests were calculated and compared.

4.1   Introduction

Micropiles are a type of deep foundation with small diameters normally less than 300 mm. They were first introduced in the 1950s by Fernando Lizzi to underpin damaged historic buildings in Italy (Bruce 1988). Micropiles are bored, grouted piles that are typically reinforced with steel cages (FHWA 2005). Micropiles serve as an alternative to conventional driven piles or drilled shafts when there are difficult ground conditions such as the limited access to construction sites. Because of the relatively small size, the equipment required for pile installation is also smaller and the installation is relatively quicker than conventional piles. The micropile technique was quickly adopted and the engineering applications has evolved to include seismic retrofitting, in-situ soil reinforcement, and underpinning existing foundations.

With the increasing demand on grouted micropile technology, many studies have been carried out on the performance of micropiles subject to axial loadings to understand the load-transfer mechanism and to develop effective design methods for micropiles. Bruce and Yeung (1984) stated that the geotechnical capacity of micropiles is dictated by the shear resistance at the grout / ground interface and settlements of 10% to 20% of the pile diameter is required to mobilize the pile capacity. Juran et al. (1999) and Cadden et al. (2004) found the key contributor to the micropile capacities was the skin friction, and the toe bearing resistance of micropiles were negligible due to the small toe area. Han and Ye (2006) carried out a field study of single micropiles in soft clay under compression or tension and concluded that the ultimate compressive skin friction for micropiles was 0.9 to 1.2 times the undrained shear strength.

A new generation of micropiles, termed ground screws, have been recently introduced to the deep foundation industry of North America. It is a steel threaded micropile, consisting of a smooth cylindrical segment on the top, a threaded cylindrical segment in the middle, and a threaded tapered segment at the bottom. Unlike drilled, grouted micropiles, this pile type does not require any grouting or reinforcement and hence can substantially reduce the construction time and cost. It is made of steel with a galvanized coating for the increased durability. This micropile is screwed into the ground under torques. Guo and Deng (2016a) carried out the field investigation of the performance of steel threaded micropiles under monotonic axial compression and tension in cohesive soil and revealed the load-transfer mechanisms along the pile shaft.

There is very limited research on the performance of micropiles subject to axial cyclic loads. Many structures such as transmission towers, solar system panels, and offshore platform are supported on pile foundations or pile groups; they are often subjected to cyclic environmental loads such as the wind, waves, and earthquakes in both the axial and lateral directions (El Naggar and Wei 2000). It is acknowledged that the response of micropiles to cyclic loads is complex (Chan and Hanna 1980) and hence the site-specific field tests may be necessary for the investigation of the soil-pile interaction under the cyclic loadings. Poulos and Sim (1990) conducted a theoretical analysis of five different "engineered" pile types and concluded that a pile taper could have a favorable effect on its cyclic performance as it reduced the stress concentration. El Naggar and Wei (2000) investigated the effect of the tapered shaft on the cyclic response of model tapered piles loaded axially in sand; they found that the pile stiffness increased with the number of load cycles, given that the load amplitude did not approach the uplift capacity of the pile. Cavey et al. (2000) studied the pressure-grouted micropiles in loose to medium dense sand and observed that there was a 60% reduction on ultimate capacity for piles

after being subjected to cyclic loading. Abd Elziz and El Naggar (2012) and Drbe and El Naggar (2015) observed no change or a slight increase in the pile head stiffness after 15 axial load cycles of hollow core micropiles installed in cohesive soils. In summary, most of the published literature is dedicated to the cyclic behavior of grouted micropiles for the soil-pile interaction is governed by the grout – ground interface, but the response of the steel threaded micropile to the axial cyclic loading has not been studied.

The present research investigates the responses of steel threaded micropiles under the monotonic and cyclic loadings in the axial direction. Six types of full-scale steel threaded micropiles were tested at a cohesive soil site located in Sherwood Park, Alberta, Canada. A comprehensive site investigation program prior to the field tests was carried out to determine the soil physical and mechanical properties. Each pile type was tested under the monotonic axial compression and axial tension. Three pile types were tested under cyclic compression loads that simulate the earthquake loads of about 0.4 g peak vertical acceleration. One micropile was instrumented with five strain gauge stations along the pile shaft and the results of this pile were discussed in detail. The results of monotonic and cyclic loading tests of the three pile types were discussed and compared in detail. The objectives of the present research are to: (1) evaluate the load-displacement behavior of steel threaded micropiles subject to monotonic axial loads, (2) determine the load distribution of micropile subject to monotonic axial loads, (3) investigate the effects of axial cyclic loadings on the load distribution, unit shaft resistance, and pile head stiffness; and (4) compare the performance of the micropiles subjected monotonic and cyclic loadings. Details of the field test program and results are presented in the test report (Guo and Deng 2016b). The present research is one part of the broader research program that is aimed at the axial and lateral behavior of steel threaded micropiles.

4.2   Site Investigation

The site, located in Sherwood Park, Alberta, Canada (as shown in Figure 4-1a and b), is part of the proposed Clover East Industrial Park that was backfilled and regraded prior to the present project. The site investigation program included four intact sampling boreholes, two cone penetration tests (CPT) within the testing area, and laboratory tests of the intact soil samples. Locations of the boreholes and CPT are shown in Figure 4-2. CPTs were performed to a depth of 5.6 m below ground surface. Borehole 1 and 2 (BH-1 and BH-2) were performed to a depth of 3.6 m; borehole 3 and 4 were drilled beside the CPT to the depth of 2.4 m.

The CPT data were processed to determine the tip resistance q_t and sleeve friction f_s and to estimate the undrained shear strength s_u of the in-situ soil. The CPT results are shown in Figure 4-3. Based on the CPT soundings and another site investigation report (Opus Stewart Weir Ltd. 2013), we revealed that this site is composed of a layer of surface backfilled silty clay, underlain by a thin layer of hard silty sand and sandy silt, underlain by cohesive backfill (CL lean clay) of about 2.0 m thickness, and then underlain by a thick layer of very stiff clay till at the depth of 2.5 m. No apparent groundwater table was detected from the CPT or the boreholes. The longest pile tested in this site was 3 m in length, and so the majority of the pile length fell in the lean clay layer.

Intact soil samples obtained from the four boreholes were tested for physical and mechanical properties. The moisture contents and bulk densities were measured immediately after the intact samples were extruded from the tubes. Figure 4-4 shows the results of moisture content, plastic limit, and liquid limit of BH-2 and BH-4. The moisture contents were shown to be greater than the plastic limit and less than the liquid limit. Liquid limit and plasticity index of soil samples from BH-1 (at depth 0.6 m), BH-2 (at depth 0.6 m, 1.8 m and 3 m) and BH-4 (at depth 0.6 m and

1.8 m) are shown on the plasticity chart in Figure 4-5; it is seen that the soil samples are inorganic clays of low to medium plasticity, or CL. Figure 4-6 Shows the saturation and void ratios of the BH-1 and BH-3 samples. The undrained shear strength s_u of the intact soils were measured using laboratory unconfined compression tests.

The CPT data were processed and estimated values of undrained shear strength s_u of the soil were calculated using Equation 1 (Robertson and Cabal 2012):

$$s_u = \frac{q_t - \sigma_v}{N_{kt}}$$

(1)

where qt is the corrected cone resistance, σv is the total vertical stress, and Nkt is the site-specific cone factor. In the present research, Nkt of 14 is adopted.

Figure 4-3 shows the s_u estimated from the CPT results and the su measured from unconfined compression tests. It is apparent that the lab results agree reasonably well with the in-situ results over the cohesive backfill layer. It is therefore concluded that the soil where test micropiles were embedded was medium-stiff silty clay with an approximate s_u of 80 to 100 kPa. The skin resistance f_s of the CPT soundings shows that the soil backfill lean clay CL has a high remolded strength ranging from 50 to 100 kPa, which is comparable to the peak s_u; this is reasonable given that the soil in this layer is newly consolidated and has not undergone any mechanical preloading or cementation. Figure 4-2 shows that the instrumented pile at this test site was located near BH-1 and BH-2; as a result, the soil properties used in data analysis was adopted from lab test results of BH-1 and BH-2.

4.3 Field Test Program

The field load tests were carried out from November 7 to December 9, 2015, when the ground surface was unfrozen and relatively dry. The piles were tested under monotonic axial compressive and tensile loadings according to ASTM standards; or under cyclic axial compression loads that simulate the cyclic inertia forces from the superstructure during vertical ground motions.

4.3.1 Test piles and the installation

Six pile types with different sizes were selected for field tests, pile ID and detailed dimensions of each pile is listed in Table 4-1. Pile size, test ID, end installation torque (T_{end}) are instead in Table 4-2 The first part of the pile ID indicates pile number ranging from P1 to P6, and the second part represents the test type and repetition number (MC for monotonic compression, MT for monotonic tension, and CY for cyclic loading). Because test piles varied in length and diameter, the first number in the pile size represents the pile diameter along the smooth segment, and the second number represents the total length. For example, M114X3000 is the pile with a 114 mm diameter and 3000 mm total length. The pile shaft and threads are made of structural steel having a Young's modulus of 210 GPa and a yield strength of 248 MPa. The pile material conforms to the German standards DIN EN 10219-1 (DIN 2006a) and DIN EN 10219-2 (DIN 2006b).

The steel threaded micropiles were installed using the specialized equipment that applies the torques to the pile head and a small axial loading (termed the crowding loads) to assist the penetration of the pile. Figure 4-7 shows the photo of a test micropile being installed. This installation method is shown to minimize the disturbance to the surround soils, reduces the heave

of the ground surface, and therefore may increase the axial capacities. If the ground is stiff, a

pilot borehole may be drilled prior to installation of the piles to protect the shaft from structural

damages, but the pilot borehole was not used for the present research. Due to the imperfect

verticality during the installation and the shaft diameter variation, an annular cavity may be

sometimes observed around the pile shaft at the ground surface to decrease the shaft resistance

near the ground surface.

4.3.2   Loading frame and instrumentation

Figure 4-8 shows the schematic and photo of the load test apparatus designed following

ASTM D1143 (ASTM 2007a) and D3689 (ASTM 2007b) with minor revisions. The loading

frame consists of a 4.2 m long W360X179 I-beam and a group of four 2.1 m long reaction piles

with a diameter of 140 mm on each end of the beam. The reaction pile groups and the beam are

connected by pile caps, threaded steel bars and plates. Two linear potentiometers (LP) and one

load cell was attached to the hydraulic jack to measure pile head displacement and applied load.

A built-in sensor in the driver head measured and recorded the end installation torque (T_{end}). One

pile (P6) was instrumented with five strain gauge stations across the pile length. The strain

gauges were applied onto the external surface of the pile (Figure 4-9a), and protected by three

layers of coatings: epoxy (Figure 4-9b), aluminum foil tape with a rubber seal on the edge

(Figure 4-9c), and plastic tapes (Figure 4-9d). The epoxy coating holds the gauge and wire in

place, rubber coating can stop water and soil from getting into the circuit and the tapes provide

protection from physical damage. The protective measures were proven to be effective at this test

site because all strain gauges survived after the installation.

4.3.3   Procedure of monotonic loading test

Test procedure conformed to ASTM D1143 (ASTM 2007a) for axial compressive load test and ASTM D3689 (ASTM 2007b) for axial tensile load test. Procedure A: Quick Test in the ASTM standard was adopted. The capacity of the test pile was estimated based on the previous load tests of similar pile types. The load was applied at an increment of 5% of the anticipated pile capacity at plunging failure; if the pile did not fail at the anticipated capacity, the load was applied in the same increment until failure. During each load interval, the load was maintained constant for 5 min. After reaching the failure, the pile was unloaded in four equal decrements.

4.3.4   Procedure of cyclic loading test

Three steel threaded micropiles were tested under one-way compressive cyclic loading to simulate the effects of seismic loading. Each pile was first loaded to 50% of its estimated limit state capacity in several increments, followed by 15 cycles of one-way compressive cyclic loading to simulate the cyclic loading typical of a M7.5 earthquake (Rollins et al. 2006, Abd Elaziz and El Naggar 2012, Seed et al. 1975). The 15 cycles were applied within 10 minutes and the load applied during each cycle ranges from 20% to 80% of the estimated limit state capacity of the test pile. Therefore, the amplitude of the axial cyclic loads was chosen to simulate a vertical ground motion of about 0.4 g. The test procedure for cyclic loading does not follow the ASTM D1143 (ASTM 2007a) cyclic loading test procedure. Although the lateral cyclic loadings due to the horizontal ground vibration during an earthquake are of vital importance, the present research has been dedicated to investigating the effects of the axial cyclic loading.

4.4   Monotonic Test Results and Analysis

After the field loading tests, piles were uninstalled by torque and examined thoroughly to check the integrity of structural steel; no visible damage was observed on the pile shaft or

threads. Figure 4-2 shows the layout of all test piles and the labels the locations of test piles for which the results will be analyzed and discussed in detail.

4.4.1 Limit state capacity, normalized displacement and end installation torque

The limit state pile capacity, Q_L, is defined as the load a pile can sustain before reaching the plunging failure (Salgado 2008). The displacement at the limit state, w_L, is the displacement of pile head corresponding to the limit state capacity. Table 4-2 summarizes the limit state pile capacity, Q_L, and the normalized displacement at the limit state, w_L/D (where D is the pile diameter of the smooth shaft). Figure 4-10a shows one loading curve for each pile type tested under compression. It was observed that for both compression and tension tests, the pile capacity is fully mobilized when the displacement is between 0.1 to 0.2 times the pile diameter, which agrees with the observation of Bruce and Yeung (1984) that axial settlements of 10% to 20% of the pile diameter are required to mobilize the pile capacity for micropiles.

For the compression test, the pile capacity and initial stiffness (slope of the linear portion of the loading curve) increases with the pile diameter and pile length. The bearing capacities of long piles (P1, P3 and P5) are much greater than that of short piles with the same diameter (P2, P4 and P6). Because P1 and P2 have a unique shape where the diameter of the pile changes twice along the length, and P5 has a shorter threaded length compared to other long piles, it is better to compare the capacity of P3, P4 and P6 to verify the influence of pile length and pile diameter on the pile capacity. P3 and P4 share the same diameter (89 mm) while P3 is 87.5% longer than P4, and the average Q_L under compression for P3 is 335% greater than that of P4. P4 and P6 share the same length (1600 mm) while the diameter of P6 is 14.6% less than that of P4, and the average Q_L under compression for P6 is only 11.6% less than that of P4. This indicates that the pile capacity of steel threaded micropiles is much more sensitive to pile length than to pile

diameter; this was also because the undrained shear strength of the soil layer deeper than 2.5 m is significantly greater than the strength of the shallower layer (shown in Figure 4-3).

As shown in Figure 4-10b, during the tension tests, the initial stiffness and pile capacity of P1 and P3 are almost identical although both greater than that of P5. This behavior is considered reasonable because even though these three long piles have the same total length, the threaded length of P1 and P3 is 1.74 times that of P5. And because threaded segment is the key contributor to the pile capacity (Guo and Deng 2017), given similar soil conditions, P6 should have a lower capacity than P3 and P1. The fact that there is no significant difference in the bearing capacities of P1 and P3 could be caused by the heterogeneity of the in-situ soil.

Because this pile type is installed under mechanical torque, the installation torque over the last cycle of rotation of the pile driver was recorded as T_{end} and listed in Table 4-2. The end installation torque can serve as an indicator of the in-situ soil strength (Guo and Deng 2017). From Table 4-2, it is observed that for the same pile type, the torque values are fairly consistent. Another finding is that with similar installation torque, compressive capacity for all test piles is greater than tensile capacity by an average of 27%.

4.4.2   Axial load distribution

Steel threaded micropiles contain three segments: smooth segment, straight threaded segment and threaded tapered segment. In order to determine the load distribution among segments of the pile, P6 was instrumented with five strain gauge stations (locations of strain gauge stations are shown in Figure 4-11). The internal shaft load Q at a strain gauge station is calculated using Equation 2:

$$Q = \varepsilon EA \tag{2}$$

where ε is the measured strain, E is the Young's modulus of the steel, and A is the cross-sectional area at the gauge station. In the tapered segment, A is revised to account for the change in wall thickness.

For the compression test P6-MC2 (Figure 4-11a), it is observed that at the limit state, the load transferred to the smooth segment is nearly zero. The majority of the load was carried by the threaded segment and the end toe bearing was negligible. The observation is consistent with the findings presented in Guo and Deng (2017). For the tension test P6-MT3 (Figure 4-11b), however, at the limit state the smooth shaft carried a significant portion (about 10 kN) of the applied pile head load (32.3 kN). From the site investigation results, the surficial 0.5 m thick soils are sandy and have a very high s_u. It is possible that the tension test P6-MT3 was located at an area where the top soils are more frictional, and therefore more load was distributed to the smooth segment. In addition, the wedge effect during pile tension tests may also increase the pullout resistance of the piles. The end installation torque for tension test P6-MT3 is 0.771 kN-m, which is 48% greater than that of the compression test P6-MC2 (0.521 kN-m). The difference in installation torques suggests the soils at the tension test location provided more resistance during the pile installation and the pull-out test.

4.4.3 Unit shaft resistance development

In order to understand the load transferred to the soil at various segments, the unit shaft resistance at limit state, q_{sL}, is calculated using Equation 3:

$$q_{sL_{ij}} = \frac{Q_{Li} - Q_{Lj}}{S_{ij}} \tag{3}$$

where q_{sLij} is the unit shaft resistance between adjacent strain gauge Station i and Station j, Q_{Li} is the measured internal load at the limit state at Station i, and S_{ij} is the surface area of the shaft segment between Station i and Station j. Note that for threaded segments, the thread width was accounted for when calculating the surface area of the pile.

For the pile loaded under compression (as shown in Figure 4-11a), q_{sL} is at the lowest along the smooth shaft (close to zero), is higher along the threaded straight shaft and is the highest along the threaded tapered segment. When the pile is loaded under tension (Figure 4-11b), the same behavior was observed except that q_{sL} is 50 kPa for the smooth shaft.

The unit shaft resistance, q_s, was plotted against the normalized displacement (Figure 4-12) for the instrumented pile under both the compression and tension to further investigate the development of unit shaft resistance. In Figure 4-12a, q_s for the smooth shaft was magnified by 10 times for clarification. From Figure 4-12a, it is observed that q_s for all three segments increased rapidly with the displacement and reached the plateau when the axial displacement was 5% of the pile diameter. For the smooth shaft, q_s was mobilized before other segments (at about 3.5% of normalized displacement. In Figure 4-12b, it is observed that it takes more than 5% of normalized displacement for q_s to be fully developed during the tension test. All three curves reached the plateau when w/D exceeded 8%. Note that the unit shaft resistance shown in Figure 4-12 did not show any degradation after reaching the yield resistance, apparently because the soils around the piles had a sensitivity of about 1.

4.5   Cyclic Test Results and Analysis

Load-controlled axial cyclic load tests were performed on three micropiles P1, P3, and the instrumented P6 to investigate the effect of vertical seismic loading on the pile performance

characteristics. The test piles were first loaded under the compression to 50% of the anticipated limit capacity Q_L to imitate the ordinary operation condition, following the same procedure and increments as for the monotonic load tests. This initial axial load was corresponding to a factor of safety (FS) of 2.0 with respect to the axial failure. Then, fifteen cycles of one-way compression cyclic loading were completed within 10 minutes. For the cyclic loading tests, the maximum load applied was 80% of the anticipated Q_L, and the minimum load applied was 20% of the anticipated Q_L; in other words, the amplitude of the cyclic load was 30% of the anticipated Q_L. As a result, the FS would be changed from 1.25 to 5. The actual amplitude of the applied load may be deviated from the designed amplitude, due to the sensitivity of the hydraulic jack and effects of manual operation. The response of test piles was examined by measuring the load applied at the pile head and the displacement of the pile head at each cycle. Figure 4-13 shows the time histories of the axial load and pile head displacement for all three cyclic tests.

Figure 4-14 shows the time histories of strain gauge measurements of the test P6-CY1, emphasizing on the cyclic loading period. Locations of strain gauges are shown in Figure 4-11. It was observed that the loads measured by most each gauge bounced up and down from the baseline; the load measured by SG-5 did not show typical cyclic behaviour around the baseline, which may be caused by a glitch in the gauges. The purpose of SG-5 is to capture the toe-bearing effect of the steel threaded micropiles. At the initial stage (right before cyclic loading starts), the applied load was approximately 20 kN and the load measured at SG-5 was about 2 kN, which is 10% of the applied load. However, at the end of the 15 cycles, the applied load was 10 kN while the measured load at SG-5 was only 0.5 kN, which is 5% of the applied load. It was already established that the pile capacity of micropiles is dictated by skin friction, and the toe-bearing is

negligible due to the small diameter of the pile toe. Figure 4-14 also shows that a degradation of toe-bearing effect can be expected for steel threaded micropiles under axial cyclic loadings.

Figure 4-15 shows the cyclic load-displacement response of P1, P3 and P6. For all test piles, the pile head movement increases with the number of load cycles. After 15 cycles, the cumulative pile head displacements were 1.68 mm, 1.40 mm, and 1.21 mm, for P6, P3, and P1, respectively. The cumulative pile displacements were considered acceptably small, given the ranges of the pile shaft diameter. P3 and P1 have the same pile length of 3 m, but the diameter of P1 is 28% higher than P3. The results indicate that given the same pile length, the pile with a greater diameter will undergo less settlement under the cyclic loading pattern.

4.5.1   Load distribution and unit shaft resistance

For the test P6-CY1, the differential loads measured between strain gauge stations are useful to inspect the distribution and the redistribution of the loads transfer through the shaft. Figure 4-16 shows the loads measured by strain gauges versus the applied pile head load for test P6-CY1. The results were smoothed for a better presentation. At the beginning of the cyclic loading, the applied load was 18.5 kN. The anticipated axial compressive pile capacity of P6 is 30 kN, and therefore the initial factor of safety (FS) is 1.6. In Figure 4-16, the vertical lines refer to the factors of safety corresponding to the applied pile head loads Q. It is shown in Figure 4-16 that: the curves of SG-1 and SG-4 did not show any change in the slopes during the cyclic loading, but SG-2 to SG-3 did. At the minimum pile head loads (FS = 2.8), SG-2 and SG-3 measured an axial load that is considerably greater than would be in the monotonic loading stage; in other words, the percentage of axial loading carried by the pile segments between SG-1, SG-2, and SG-3 have been changed over the cycles. This trend indicates that cyclic loading might have redistributed the load transfer along the pile shaft.

To further investigate the load redistribution, the measured axial loads at following five stages were chosen and compared: the initial (prior to cyclic loading), the maximum and minimum in the first cycle, and the maximum and minimum in the last (15th) cycle. Table 4-3 summarizes the percentage of applied loads carried by each pile shaft segment defined by the strain gauge stations. Threaded shaft 1 is between SG-2 and SG-3, which has the same shape (threaded and straight) as threaded shaft 2 (between SG-3and SG-4) but 50 mm longer. From Table 4-3, the load distribution at the initial stage is only 2% different from that when the pile is loaded to maximum during 1st and 15th cycle, which means the load distribution did not change significantly during the continuing loading stage. At the minimum of the 1st and 15th cycle, however, the load carried by the smooth shaft segment is negative, implying a negative skin friction along the smooth shaft of the pile given the relaxation of the axial loading. The negative skin friction was because when the axial load decreases, the soils experienced relaxation and the pile slightly rebound. The upward movement, although very small, can introduce negative skin friction to the smooth shaft. When the pile head load was at the minimum of the 1st and 15th cycle, the percentage of the load carried by threaded shafts 1 and 2 increased to counterbalance the negative skin friction. There is no clear trend for the load distribution change along the tapered shaft.

Figure 4-17 shows the distribution of the unit shaft resistance, q_s, of the test P6-CY1 along the pile shaft. Similar to Table 3, the q_s distribution was captured at the initial stage and at the maximum and minimum of the 1st and 15th cycle. When the load is at the minimum of the 1st and 15th cycles, a negative skin friction of about -7.8 kPa was developed along the smooth shaft. Because there are limited numbers of strain gauge stations, the exact location of the neutral plane where negative skin friction transitions from the negative to the positive cannot be determined.

At the maximum of the loading cycles, the skin friction in the smooth shaft segment increased to 10 to 12 kPa that is slighted greater than the resistance of 6 kPa at the initial stage. At the initial stage when the axial displacement was only 1 mm, the q_s along the threaded segments was 54 kPa, 63 kPa, and 90 kPa only, which were less than the q_{sL} measured from monotonic compression tests and had not been fully mobilized yet. When the load reaches the local high point of the first and 15th cycle, q_s for all pile segments increased and the distribution curves shifted to the right as shown in Figure 4-17. When the load was at maximum during the 1st and 15th cycle, q_s for the threaded shaft 2 is very close to undrained strength of 80 kPa, indicating the shaft resistance had been fully mobilized. During the first cycle, when the load reaches maximum (24.7 kN), q_s for the tapered shaft was 128 kPa. During the last cycle, q_s for the tapered shaft was 94 kPa when the applied maximum load was 22.5 kN. With only 9% decrease in the applied load, q_s along the tapered shaft decreased by 27%. It is possible the cyclic loading and the number of cycles had a negative impact on the performance of the tapered pile shaft.

4.5.2   Axial stiffnesses

To further examine the effect of the cyclic loading on the pile head movement, the axial stiffness, K_{cyc}, at each load cycle is calculated by the slope of the load-displacement curve during each load cycle using Equation 4:

$$K_{cyc} = \frac{Q_{max} - Q_{min}}{w_{max} - w_{min}} \qquad (4)$$

where Q_{max} and Q_{min} are the maximum and minimum applied loads at each cycle, and w_{max} and w_{min} are the corresponding pile head movements.

Figure 4-18 shows the calculated axial stiffness versus the number of cycles. It is noted that

the stiffness did not show a clear steady trend during the load cycles. The stiffness is the lowest

at the first cycle for all three tests, and it increased in some cycles and decreased in others. No

degradation of pile axial stiffness was observed for the three piles tested under the above-

mentioned range of applied magnitudes of cyclic loading. At the cyclic loading stage, the total

displacement of each pile is less than 5% of its diameter, which means the shaft resistance is not

fully mobilized yet. Given different loading sequence (i.e. if the cyclic loading starts after the

pile is loaded till displacement reaches 5% of the pile diameter), the pile axial stiffness might

change with the number of cycles.

4.5.3   Comparing cyclic and monotonic behavior

The axial stiffness and unit shaft resistance of the same pile type under monotonic and cyclic

loadings are compared in this subsection. We estimated the axial stiffness, K_{mon}, of the

micropiles tested under the monotonic loading using Equation 5:

$$K_{mon} = \frac{Q_1 - Q_2}{w_1 - w_2} \qquad (5)$$

where Q_1 and Q_2 are the applied pile head loads during the monotonic loading at certain FS

stages, and w_1 and w_2 are the corresponding pile head movements.

When P6-CY1 is loaded under cyclic loading, the FS ranges from 1.2 to 2.8. When P6-MC2 is

loaded monotonically, the FS changes from 2.8 to 1.2, the applied Q changes from 6.9 kN to

16.1 kN, and the corresponding w changes between 0.57 mm to 2.30 mm. Consequently, the

axial stiffness K_{mon} is 5.3 kN/mm. Similarly, the pile axial stiffnesses of P1 and P3 when the pile

was subjected to the same range of FS caused by 15 cycles of cyclic loading were 21.0 kN/mm and 29.3 kN/mm, respectively.

Figure 4-18 compares the calculated K_{mon} of test piles in the compression tests to the calculated K_{cyc}. It is observed that for all three test piles K_{mon} was much less than K_{cyc}. The difference in the axial stiffness could only be explained by the effect of loading rate on the soil stiffness. Therefore, it can be concluded that steel threaded micropiles under cyclic loading have a stiffer response than under monotonic loading.

Figure 4-19 shows the distribution of q_s of the test pile P6 subject to cyclic and monotonic loadings. It was observed the installation torque for these two tests are different, therefore these micropiles may potentially have different bearing capacities. Hence, instead of comparing the q_s distribution at the same applied Q, the q_s distribution at the same FS are compared. It is observed that when FS was the same, the q_s for the cyclic test were greater than for the monotonic test. A FS of 3 for the cyclic test was reached when the cyclic loadings were completed and the pile was at the first unloading stage. Therefore, there exists negative skin friction at the smooth shaft as the pile undergoes upward movements. When FS changes from 3 to 1.3, for the monotonic test, q_s increased, especially for the tapered segment. But for cyclic test (maximum load of the 15th cycle), the increase in q_s for the tapered segment is not as drastic. Even though all other segments had a greater q_s during cyclic loading, the q_s for tapered segment during cyclic loading turned out to be less than monotonic test. This confirms that the superiority of the taper shape can be compromised by cyclic loading.

As noted by prior research (e.g., Abd Elaziz and El Naggar 2012, Drbe and El Naggar 2015), the behaviour of micropiles subjected to cyclic axial loadings depend on the initial axial loading,

the amplitude and number of cyclic loading. In addition, the soil's cyclic resistance plays an important role in the axial cyclic response of the piles. It is anticipated that the behaviour of the steel threaded piles would be different if the loading pattern and soils were changed.

4.6   Conclusions

Full-scale monotonic and cyclic load tests were conducted on six steel threaded micropiles at a cohesive soil site. The diameter of test piles ranges from 76 mm to 114 mm, and the length ranges from 1.6 m to 3 m. Comprehensive site investigation was carried out and selected piles were instrumented with strain gauges. For cyclic tests, the piles were monotonically loaded to approximately 50% of the anticipated pile capacity, and then subjected to 15 cycles of one-way compressive cyclic loading that simulates a vertical acceleration of 0.4 g. Following conclusions may be drawn:

1. With the similar installation torques, the compressive capacity for all test piles is greater than the tensile capacity by an average of 27%. Long piles of 3 m length exhibited greater axial capacities than short piles of 1.5 m length, due to the existence of a stiff clay till layer at the tip of the long piles and the greater shaft surface area.

2. This micropile type behaves as friction piles. For monotonic tests, the shaft resistance of the pile is fully mobilized when the displacement reaches 5% to 10% of the pile diameter. For both compression and tension tests, the pile capacity is fully mobilized when the displacement is 10% to 20% of the pile diameter.

3. Cumulative axial displacements were observed during the cyclic loading. The magnitude of the displacement ranged from 1.21 mm to 1.68 mm and decreased with the pile length or pile diameter. The small displacements confirmed the good performance of this pile type installed in stiff cohesive clays under vertical earthquake loadings.

4. The load transfer along the pile shaft segments was redistributed during the cyclic loading; negative skin friction was developed along the smooth pile shaft when the pile underwent decreased axial loading in the loading cycles; the load transfer along the threaded shaft was nearly constant during the cyclic loading. No degradation of pile axial stiffness was observed for the three piles tested under the range of applied cyclic loading.

5. The monotonic axial stiffness was much less than the cyclic axial stiffness for the similar loading ranges, because of the effects of loading rate. At the same FS with respect to vertical capacity, the unit shaft resistance mobilized along the threaded segments in monotonic tests was generally less than the resistance mobilized in cyclic tests.

Table 4-1: Dimensions of test piles.

Pile ID	Diameter (mm)	Total length (mm)	Threaded length (mm)
P1	114	3000	2000
P2	114	1600	850
P3	89	3000	2000
P4	89	1600	850
P5	76	3000	1150
P6	76	1600	850

Table 4-2: Summary of the end installation torques, limit state bearing capacities, and normalized displacements at the limit state.

Pile Size	Test ID	T_{end}	Q_L	w_L/D
		(kN-m)	(kN)	(%)
M114X3000	P1-MC1	3.610	146	17
	P1-MC2	3.898	148	24
	P1-MT1	3.989	109	9
	P1-MT2	4.103	108	13
	P1-CY1	3.060	N/A	N/A
M114X1600	P2-MC1	1.314	41	10
	P2-MC2	1.405	40	18
	P2-MT1	1.314	28	8
	P2-MT2	1.314	27	6
M89X3000	P3-MC1	2.720	129	15
	P3-MC2	2.856	132	16
	P3-MT1	2.787	104	12
	P3-MT2	2.792	109	12
	P3-CY1	2.743	N/A	N/A
M89X1600	P4-MC1	0.907	32	10
	P4-MC2	0.957	28	16
	P4-MT1	1.020	28	19
	P4-MT2	0.952	16	17
M76X3000	P5-MC1	1.680	79	26
	P5-MC2	2.089	109	17
	P5-MT1	2.289	88	16
	P5-MT2	2.131	85	18
M76X1600	P6-MC1	0.612	27	12
	P6-MC2 [1]	0.521	26	15
	P6-MT1	0.545	27	13
	P6-MT2	0.634	21	25
	P6-MT3 [1]	0.771	34	17
	P6-CY1 [1]	0.612	N/A	N/A

Note: 1. The test pile was instrumented with five strain gauge stations.

Table 4-3: Load distribution in percentage of the pile head load Q at various loading stages.

Loading stage	Pile shaft segment			
	Smooth shaft	Threaded shaft 1	Threaded Shaft 2	Tapered shaft
Initial [1]	4%	34%	32%	19%
1st Max.	6%	34%	32%	21%
1st Min.	-9%	38%	41%	16%
15th Max.	5%	33%	33%	17%
15th Min.	-9%	37%	33%	17%

Note: 1. The initial stage refers to the end of the monotonic loading and the beginning of cyclic loading.
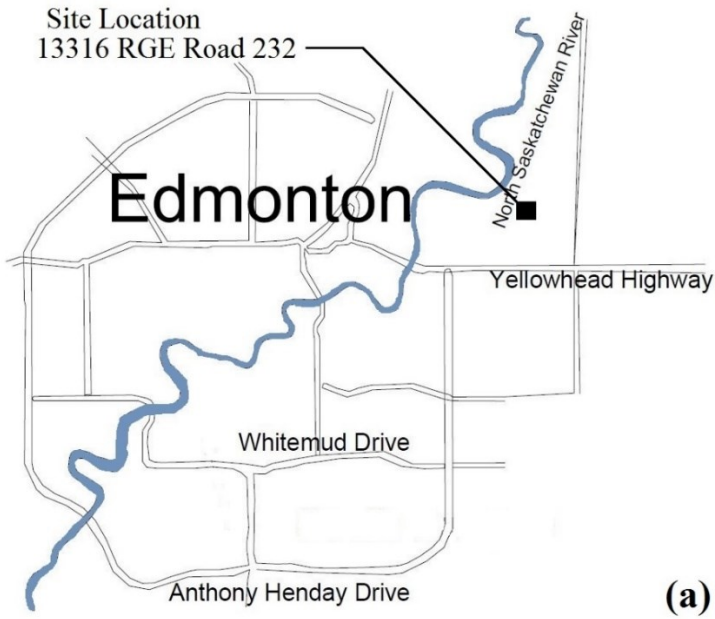
Figure 4-1: Location of the test site Sherwood Park, Alberta, Canada. Global coordinate of test site: N 53.593702, W 113.291912: (a) test site location in the map of Edmonton and (b) an overview of the test site.
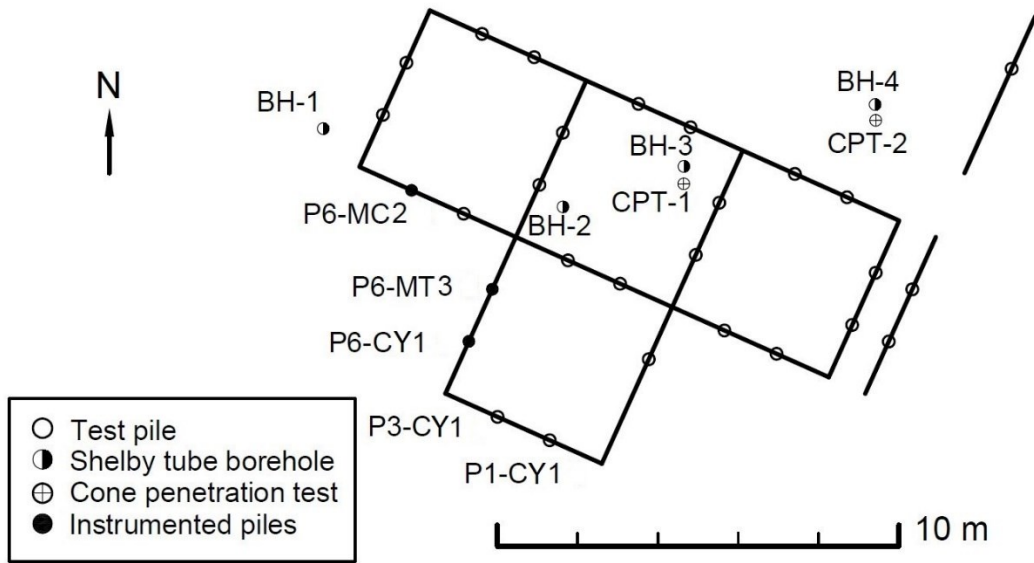
Figure 4-2: Layout of CPT, intact soil sampling boreholes (BH), and test piles.
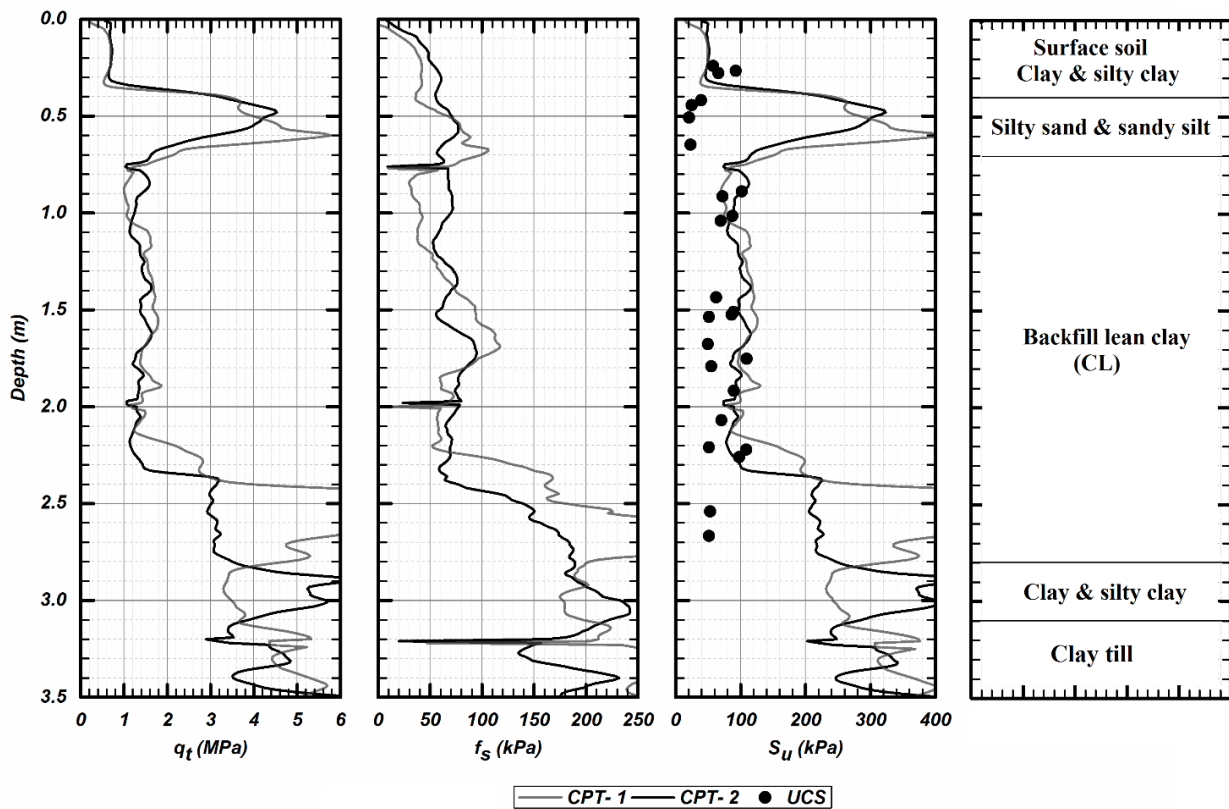
Figure 4-3: CPT test results and undrained shear strength measured in laboratory.
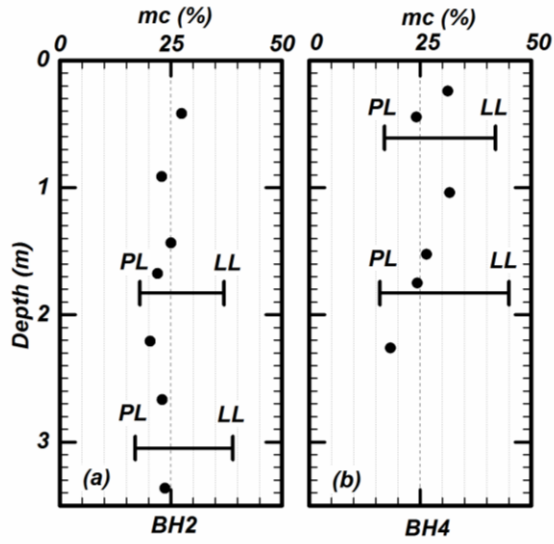
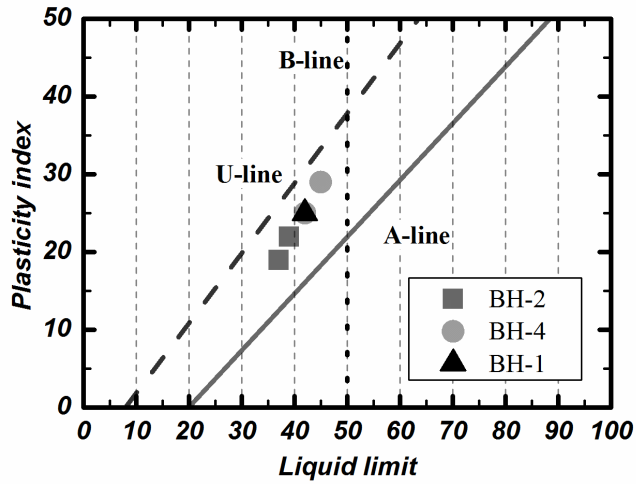Figure 4-4: Atterberg limit and natural moisture content (mc) of intact soil samples: (a) BH-2 (b) BH-4.

Figure 4-5: Plasticity chart for undisturbed soil samples from BH-1, BH-2, and BH-4.
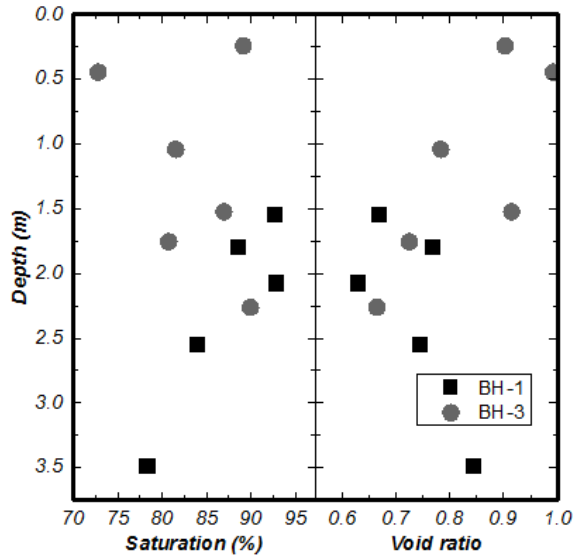
Figure 4-6: Saturation and void ratio versus depth at BH-1 and BH-3.
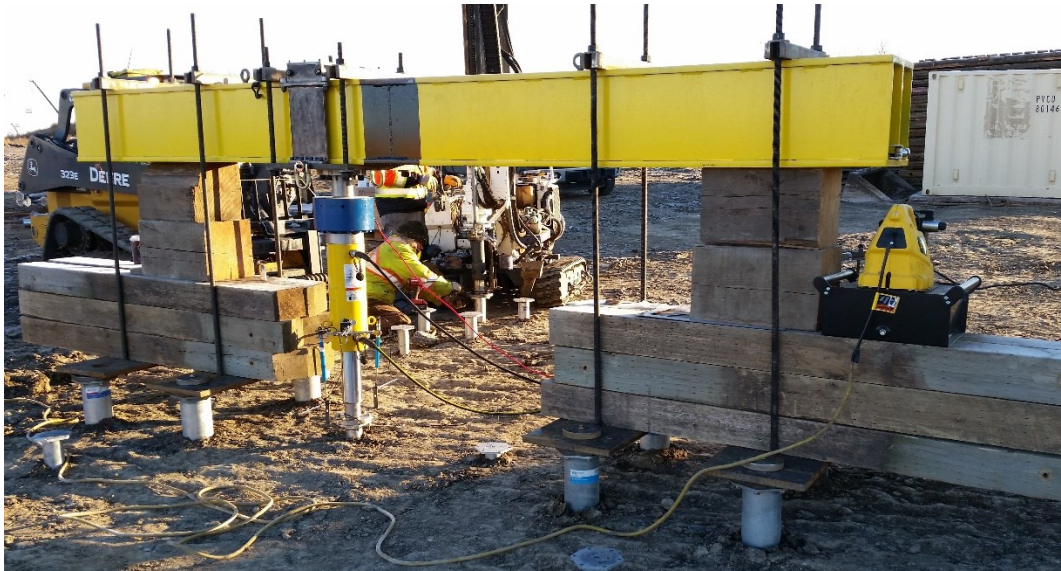

Figure 4-7: Photo of a steel threaded micropile during installation.
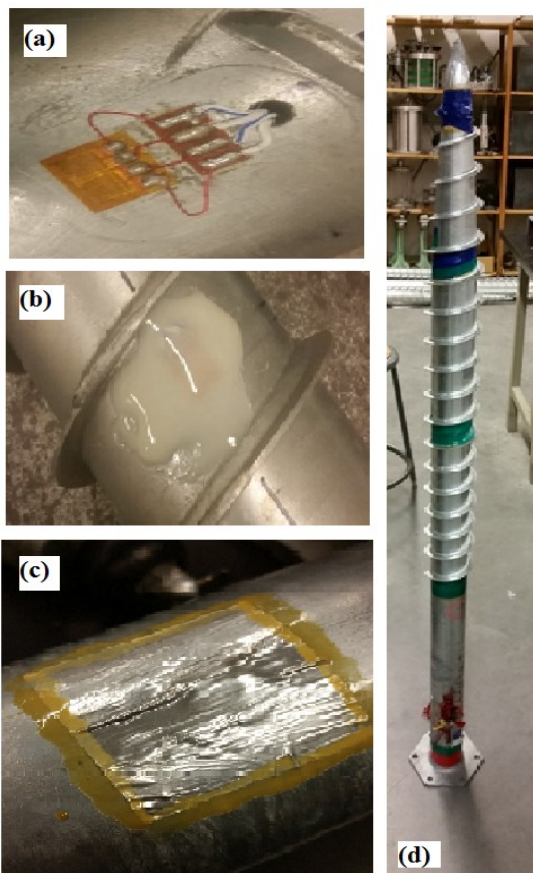
Figure 4-8: Photo of the load test apparatus.

Figure 4-9: Strain gauge installation and protection measures: (a) strain gauge, terminals and wires, (b) epoxy coating, (c) aluminum foil tape and rubber seal and (d) plastic tape on five stations.
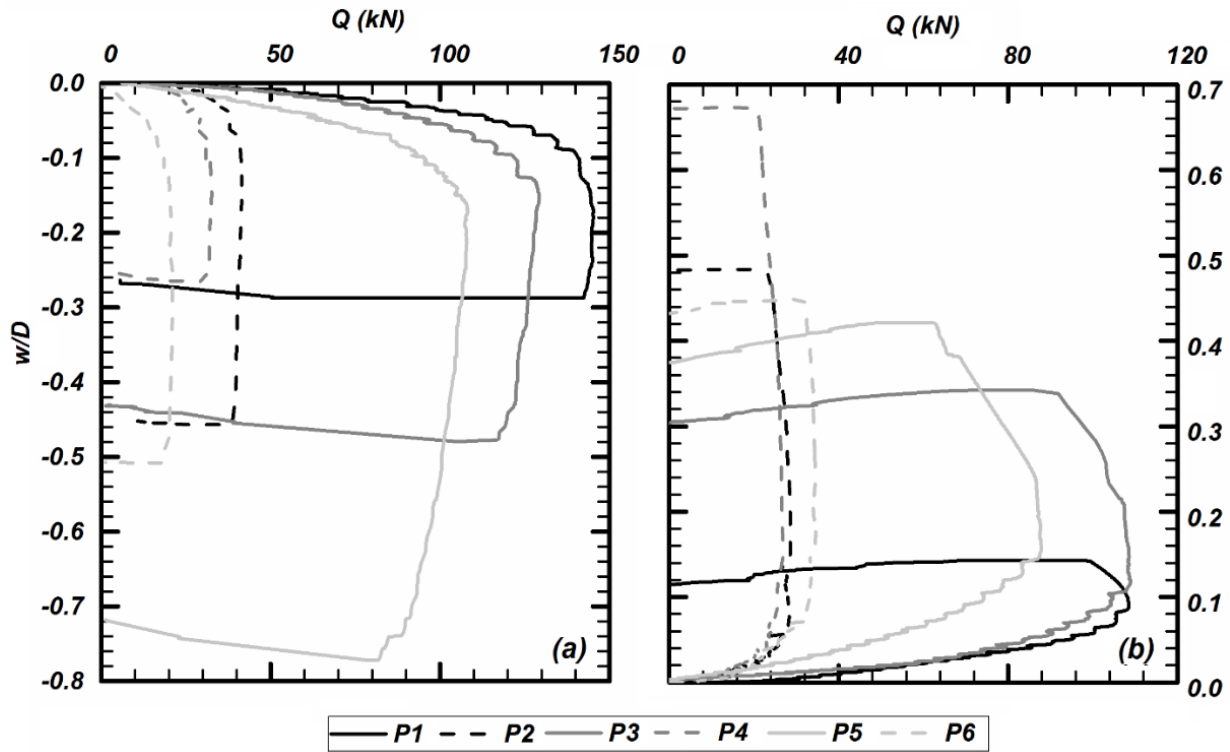
Figure 4-10: Selected axial load (Q) versus normalized axial displacement (w/D) curves for: (a) compression tests and (b) tension tests. D: diameter of pile shaft.
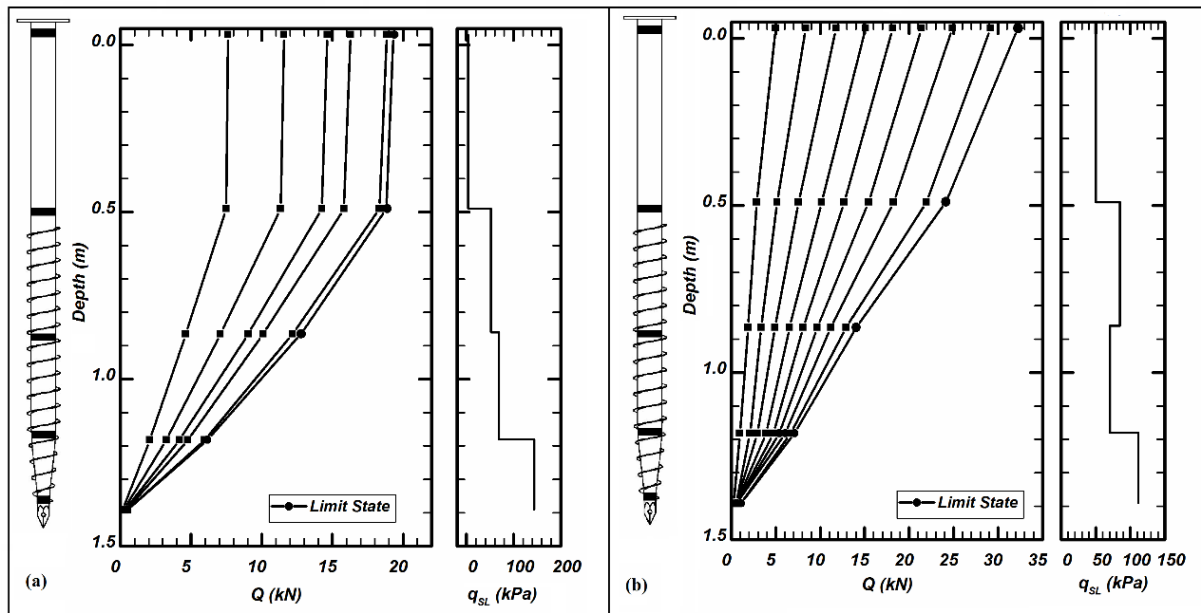

Figure 4-11: Axial loads transferred to pile shaft and unit shaft resistance at limit state (q_{sL}) for: (a) P6-MC2 and (b) P6-MT3.
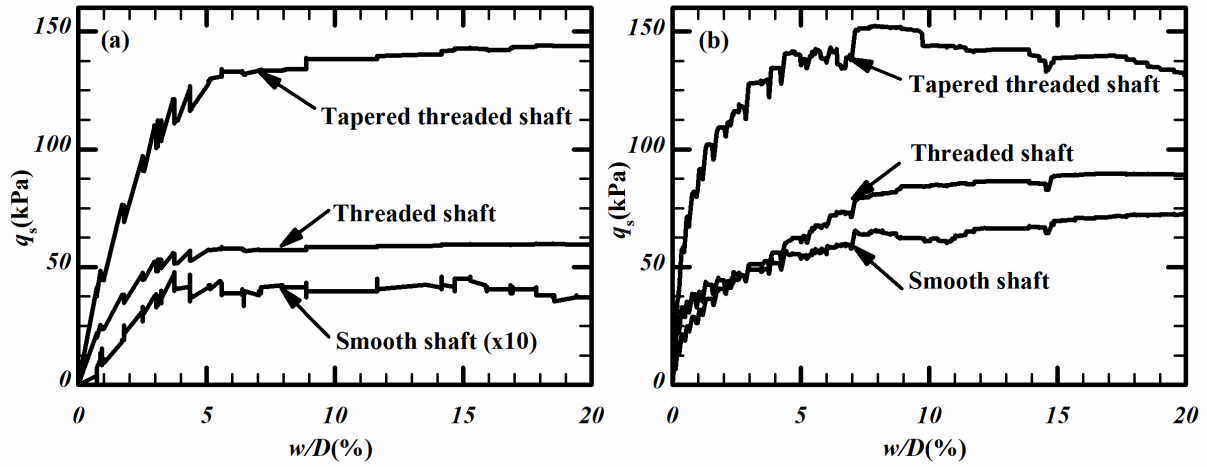
Figure 4-12: Development of unit shaft resistance q_s versus normalized axial displacement w/D for: (a) compression test P6-MC2 and (b) tension test P6-MT3.
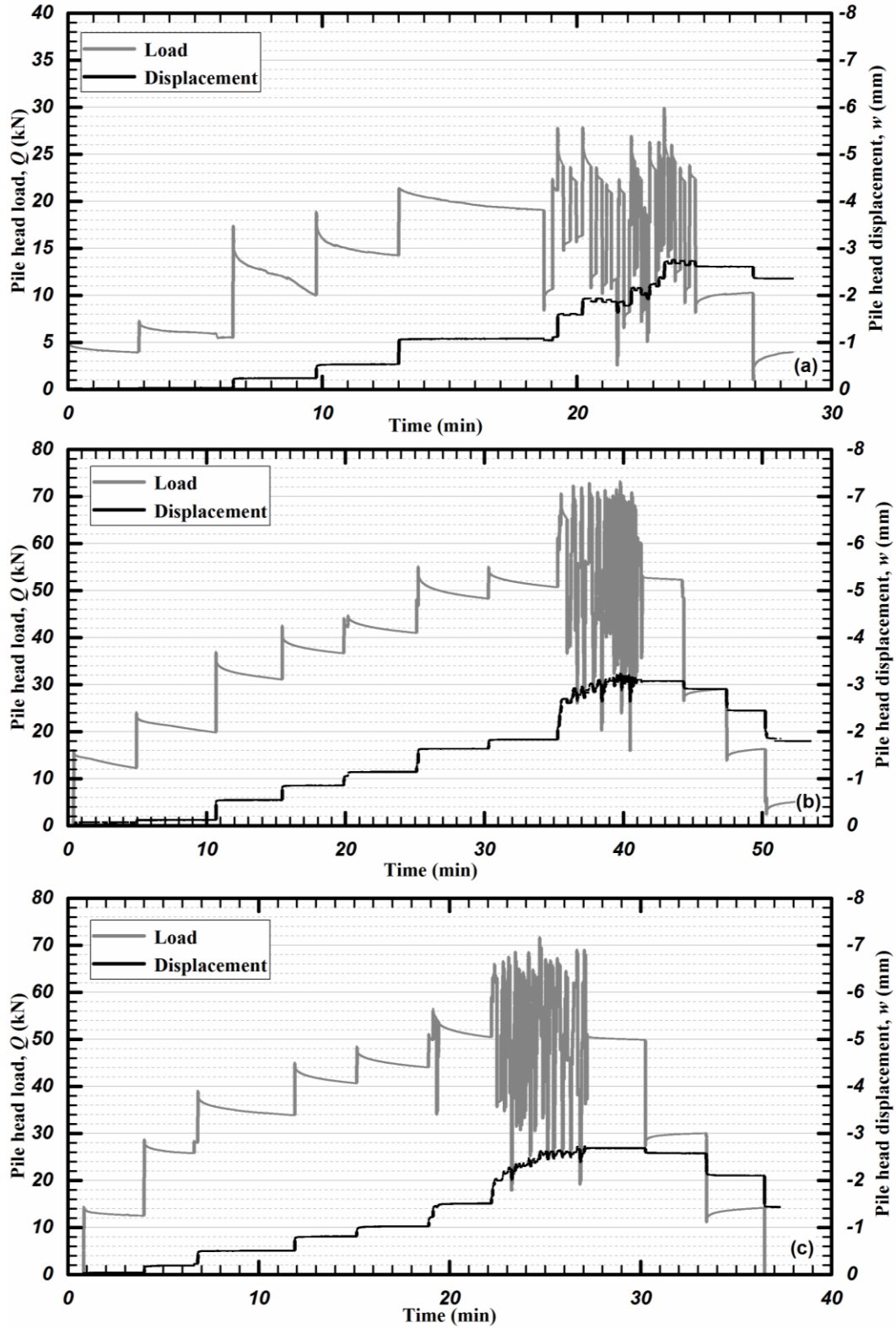
Figure 4-13: Time history of pile head load and head displacement of the cyclic compression tests of: (a) P6-CY1, (b) P3-CY1, and (c) P1-CY1.
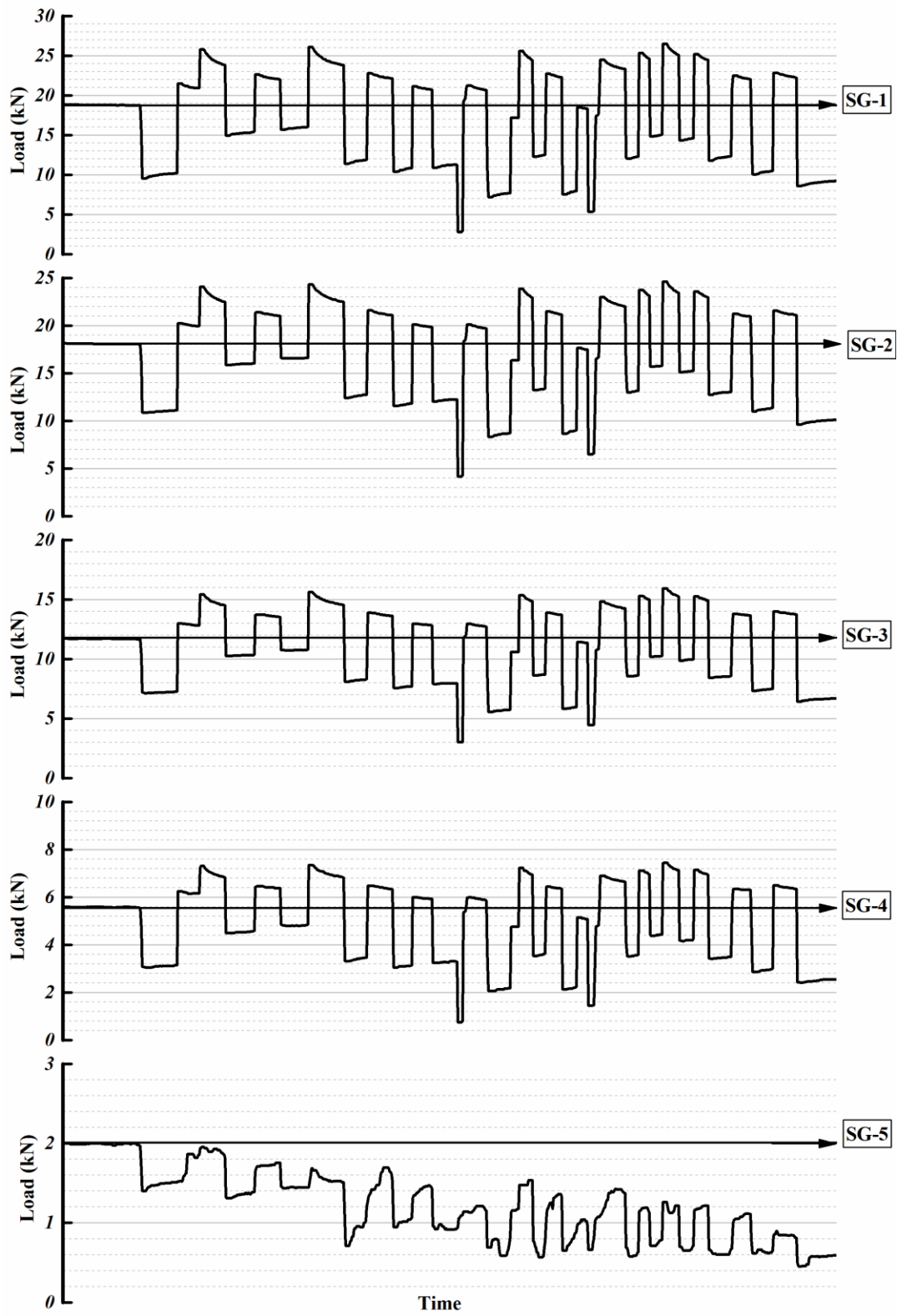
Figure 4-14: Time history of shaft internal load measured by strain gauges for test P6-CY1.
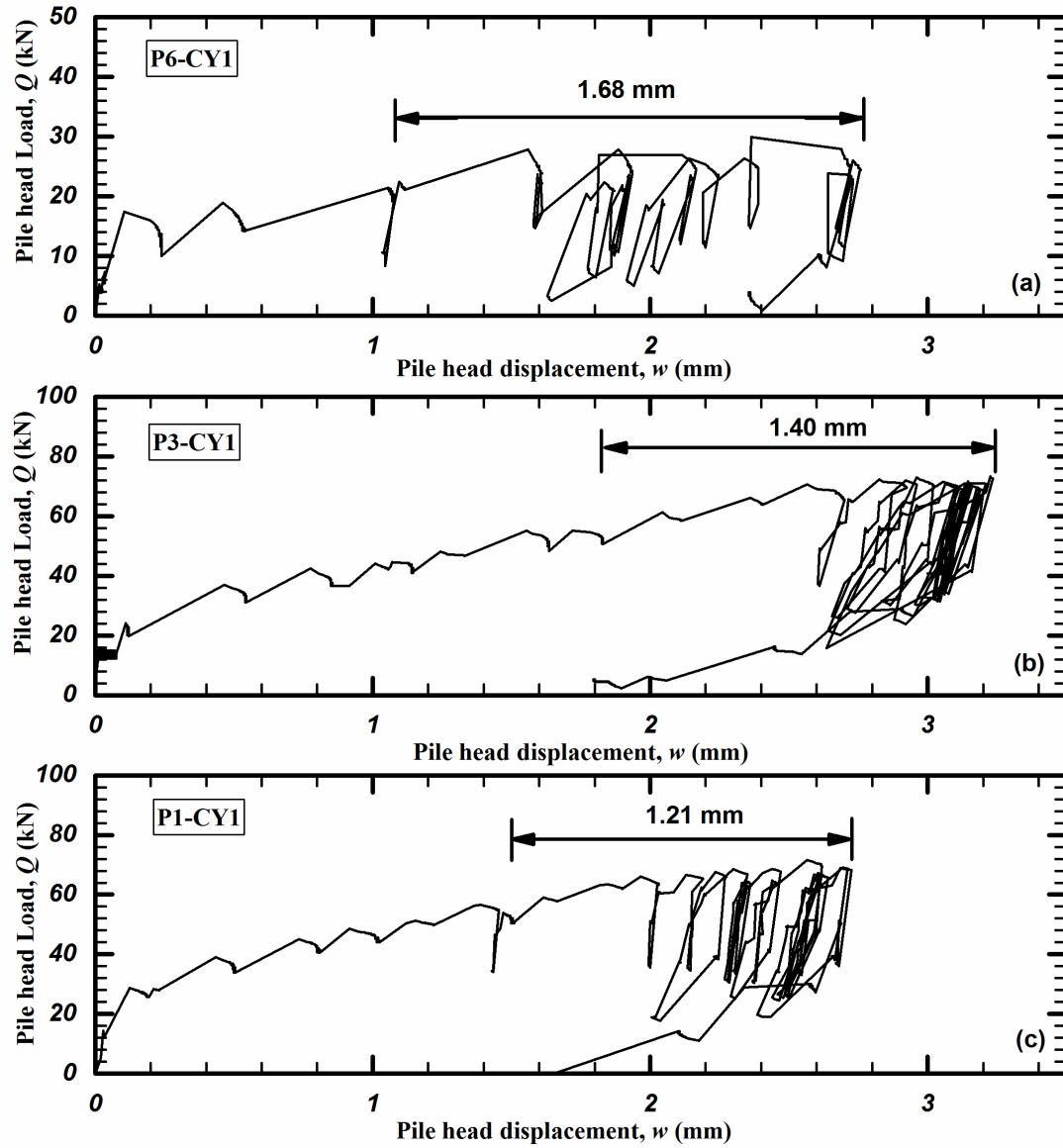
Figure 4-15: Load-displacement curve for: (a) P6-CY1, (b) P3-CY1 and (c) P1-CY1.
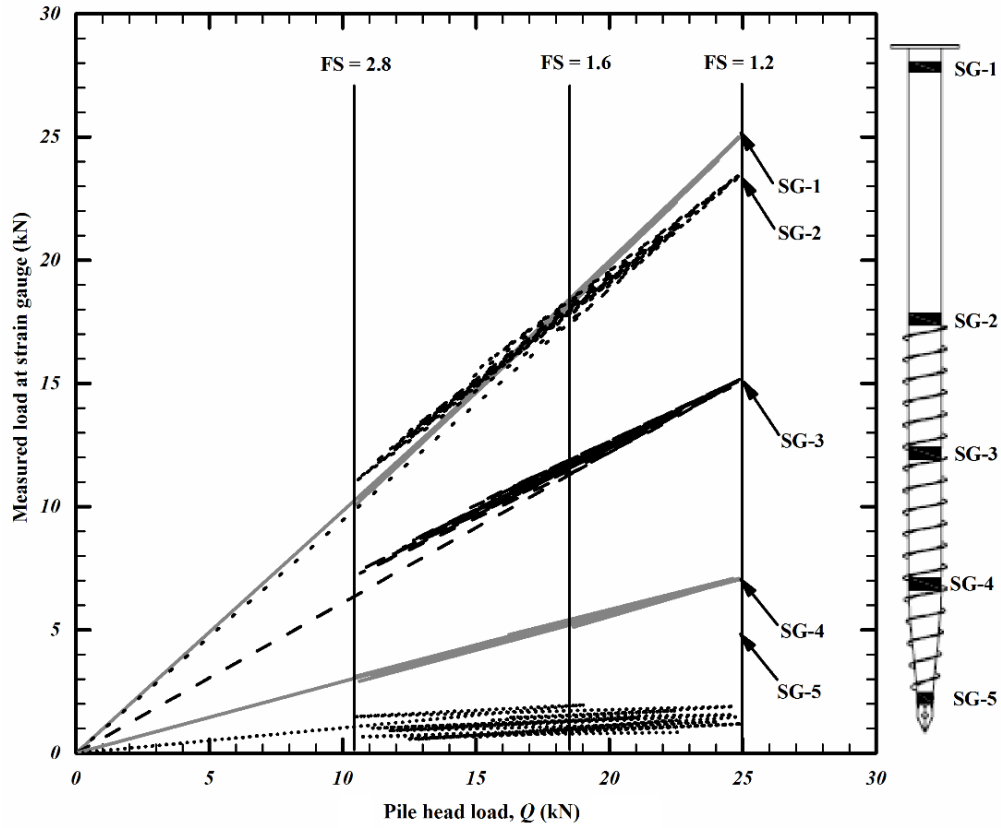
Figure 4-16: Measured loads at strain gauges versus the applied load at pile head for test P6-CY1 subjected to axial cyclic loading.
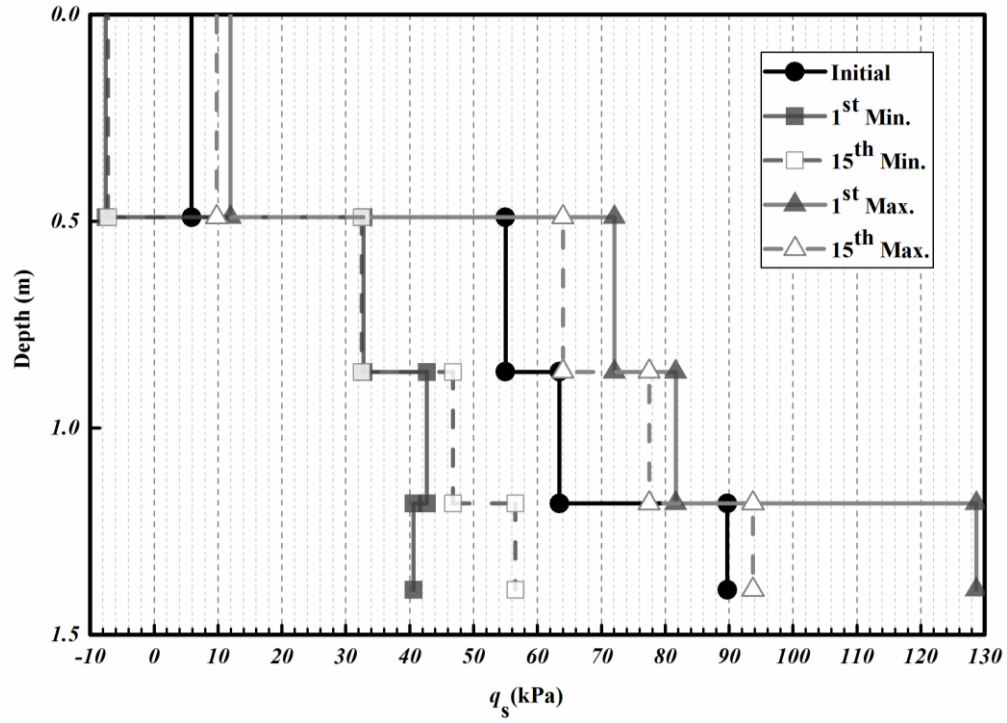
Figure 4-17: Unit shaft resistance distribution at selected cycles for test P6-CY1 subject to axial cyclic loading.
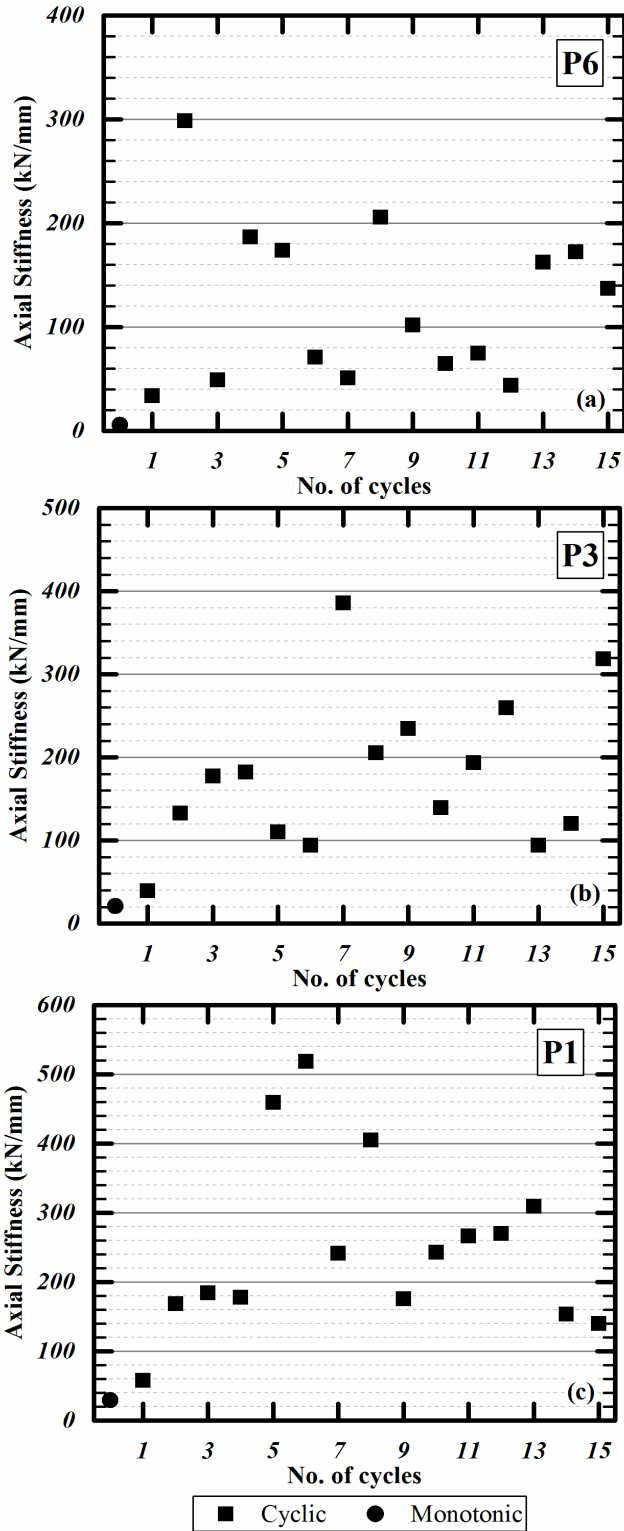
Figure 4-18. Axial Stiffness vs. number of cycles for tests: (a) P6-CY1, (b) P3-CY1 and (c) P1-CY1. The monotonic axial stiffness is the ratio of the change in applied load and the change in the corresponding displacement at certain FS stages during monotonic loading.

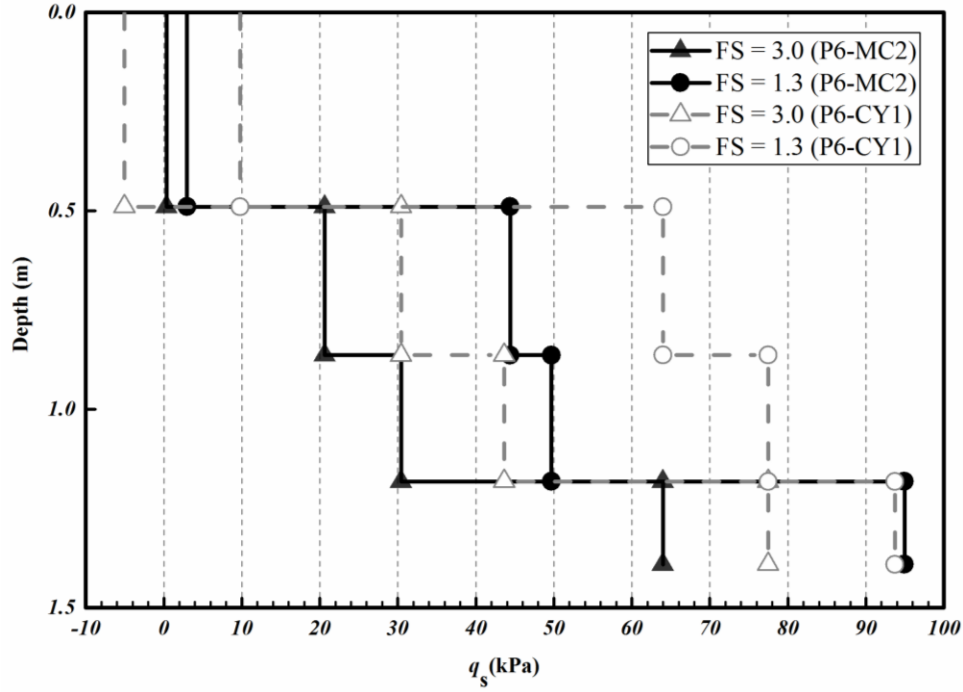Figure 4-19. Unit shaft resistance distribution at selected FS for test P6-CY1 (cyclic) and P6-MC2 (monotonic). In P6-CY1, FS equals 3 was reached at the end of the 15th cycle and FS equals 1.3 was reached at the maximum load of the 15th cycle.

5   Conclusions

Full-scale pile load tests were conducted on six steel threaded micropiles at two cohesive soil sites to evaluate the performance of steel threaded micropiles subject to axial monotonic and cyclic loadings. The micropiles consist of hollow steel shaft with threads welded onto the lower segment and a tapered pile tip. The diameter of test piles ranges from 76 mm to 114 mm, and the length ranges from 1.6 m to 3 m. Comprehensive site investigations were carried out at both sites and selected piles were instrumented with strain gauges. Following conclusions may be drawn.

5.1   Axial monotonic behavior of steel threaded micropiles

1. With the similar installation torque, the compressive capacity for all test piles is greater than tensile capacity by an average of 27%. The pile length, especially the threaded length, has a more significant impact on the pile capacity than the pile diameter. Given the same length, a pile with a greater diameter tends to have a greater axial capacity, and has a stiffer behaviour. Given the same diameter, longer piles tend to have a greater axial capacity and a greater stiffness.

2. The majority of the axial load is transferred through the shaft resistance. Most of the limit load was carried by the threaded segment. The adhesion coefficient between smooth shaft and soil is lower than 0.1 on average because the torsional installation process expands the soils and created annular gaps between pile shaft and surface soils.

3. For monotonic tests, the shaft resistance of the pile is fully mobilized when the displacement reaches 5% to 10% of the pile diameter. For both compression and tension tests, the pile capacity is fully mobilized when the displacement is 10% to 20% of the pile diameter.

4. Soils around the straight threaded segment fail in the cylindrical shear mode at the limit state. The ratio of thread spacing to thread width is 4.2 for all test piles. The presence of threads pushes the shear failure plane outward to the edge of the threads and thereby substantially increases the limit capacity of the threaded segment. The estimated limit capacities of the threaded segment based on the CSM assumption well predicted the measured capacities of instrumented piles.

5. Taper shape increases the shaft resistance. For the instrumented test piles with 5.2° and 5.5° taper angle at the tip, the limit shaft resistance of the tapered segment, is 43% on average greater than that of a cylindrical, equivalent straight shaft with the same shaft volume.

6. Limit capacities of all test piles under compression were estimated using proposed adhesion coefficient, failure mechanism, and empirical relationship between tapered segment pile capacity and straight segment pile capacity. The estimated limit capacities of piles were 12% on average less than the measured capacities. Given the complexity of field tests and soil heterogeneity, the discrepancy may be considered acceptable.

7. A theoretical torque model was proposed to estimate the end installation torque at the last cycle of rotation. The torque model considers the torque induced by the remolded shear strength acting on the shaft and the threads below the smooth segment. The torque model adopts the CPT-based sleeve friction and accounts for the site heterogeneity. The estimated torques of all test piles were 2% on average less than the measured torques, which confirms the validity of the proposed torque model.

5.2   Axial cyclic behavior of steel threaded micropiles

1. Cumulative axial displacements were observed during the cyclic loading. The magnitude of the displacement ranged from 1.21 mm to 1.68 mm and decreased with the pile length and pile diameter. The small displacements confirmed the good performance of this pile type installed in stiff cohesive clays under vertical earthquake loadings.

2. The load transfer along the pile shaft segments was redistributed during the cyclic loading; negative skin friction was developed along the smooth pile shaft when the pile underwent decreased axial loading in the loading cycles; the load transfer along the threaded shaft was nearly constant during the cyclic loading.

3. No degradation of pile axial stiffness was observed for the three piles tested under the range of applied cyclic loading. The monotonic axial stiffness was much less than the cyclic axial stiffness for the similar loading ranges, because of the effects of the loading rate. At the same FS with respect to the vertical capacity, the unit shaft resistance mobilized along the threaded segments in monotonic tests was generally less than the resistance mobilized in cyclic tests.

References

American Society for Testing and Materials (ASTM). 2007a. ASTM D1143– 07, Standard Test Methods for Deep Foundations under Static Axial Compressive Loads, West Conshohocken, PA.

American Society for Testing and Materials (ASTM). 2007b. ASTM D3689 – 07, Standard Test Methods for Deep Foundations under Static Axial Tensile Loads, West Conshohocken, PA.

Abd Elaziz, A.Y., and El Naggar, M.H. 2012. Axial behaviour of hollow core micropiles under static and cyclic loadings. Geotechnical Testing Journal, 35(2): 249–260.

Bradka, T. D. 1997. Vertical capacity of helical screw anchor piles. MEng Report, Department of Civil and Environmental Engineering, University of Alberta, Edmonton, Canada.

Bruce, D.A. 1988. Aspects of minipiling practice in the United States. Ground Engineering, 21(8): 20–39.

Bruce, D.A., and Yeung, C.K. 1984. A review of minipiling with particular regard to Hong Kong applications. Hong Kong Engineer, 12(6): 31–54.

Cadden, A., Gomez, J., Bruce, D., and Armour, T. 2004. Micropiles: recent advances and future trends. In Current practices and future trends in deep foundations. Edited by J.A. DiMaggio, and M.H. Hussein. American Society of Civil Engineers, Reston, Va., pp. 140–165.

Canadian Geotechnical Society. 2006. Canadian Foundation Engineering Manual, 4th ed., Richmond, B.C., Canada.

Cavey, J.K., Lambert, D.V., Miller, S.M., and Krhounek, R.C. 2000. Observations of minipile performance under cyclic loading conditions. Ground Improvement, 4(1): 23–29.

Chan, S.F., and Hanna, T. H., 1980, Repeated Loading on Single Piles in Sand, Journal of Geotechnical Engineering, ASCE, Vol. 106, No. 2, pp. 171–188.

Coduto, D.P. 2001. Foundation Design: Principles and Practices. Prentice-Hall Inc., Englewood Cliffs, N.J.

Cuthbertson-Black, R. 2001. The interaction between a flighted steel pipe pile and frozen sand, M.Sc. thesis, Department of Civil and Geological Engineering, University of Manitoba, Winnipeg, Manitoba.

Drbe O.F.E., and El Naggar M.H. 2015. Axial static and cyclic compression behaviour of hollow-bar micropiles. Canadian Geotechnical Journal 52(4): 426-441

Edwards, D. 1993. Gravel bar blues. In Edmonton beneath our feet. Edited by J. Godfrey. Edmonton Geological Society, Edmonton, AB, Canada.

El Naggar, M.H. and Sakr, M. 2000. Evaluation of axial performance of tapered piles from centrifuge tests, Canadian Geotechnical Journal, 37: 56-74.

El Naggar, M. H. and Wei, J. Q. 2000. Cyclic Response of Axially Loaded Tapered Model Piles, Geotechnical Testing Journal 23(1): 100 - 115

Elsherbiny, Z. and El Naggar, M.H. 2013. Axial compressive capacity of helical piles from field tests and numerical study. Canadian Geotechnical Journal, 50(12): 1191–1203.

FHWA. 2005. Micropiles design and construction. Federal Highway Administration (FHWA), U.S. Department of Transportation, Washington, D.C.

German Institute for Standardization (DIN). 2006a. DIN EN 10219-1, Cold formed welded structural hollow sections of non-alloy and fine grain steels-Part 1: Technical delivery conditions, Berlin, Germany.

German Institute for Standardization (DIN). 2006b. DIN EN 10219-2, Cold formed welded structural hollow sections of non-alloy and fine grain steels-Part 1: Tolerances, dimensions and sectional properties, Berlin, Germany.

Ghaly, A., and Hanna, A. 1991. Experimental and theoretical studies on installation torque of screw anchors. Canadian Geotechnical Journal, 28(3): 353–364.

Guo, Z., and Deng, L. 2016a. Field investigation of the behavior of tapered screw piles. Annual Conf. Can. Geotech. Society, Vancouver, B.C., pp. 8.

Guo, Z., and Deng, L. 2016b. Report of Field Load Tests of Krinner Ground-Screw Piles at Sherwood Park. Rep. No. UA/GC-D-2016/04. University of Alberta, Edmonton, AB, pp. 31.

Guo, Z., and Deng, L. 2017. Field behaviour of steel threaded micropiles subject to axial loading in cohesive soils. Canadian Geotechnical Journal (in review).

Guo, Z., Khidri, M., and Deng, L. 2017. Report of Field Load Tests of Krinner Ground Screws at the University of Alberta Farm. Rep. No. UA/GC-D-2017/01. University of Alberta, Edmonton, AB, pp. 129.

Hoyt, R. M., and Clemence, S. P. 1989. Uplift capacity of helical anchors in soil, Proceedings of the 12th International Conference on Soil Mechanics and Foundation Engineering, Rio de Janeiro, Brazil, 2: 1019-1022.

Juran, I., Bruce, D.A., Dimillio, A., and Benslimane, A. 1999. Micropiles: the state of practice. Part II: design of single micropiles and groups and networks of micropiles. Ground Improvement, 3(3): 89–110.

Kodikara, K.K. and Moore, I.D. 1993. Axial response of tapered piles in cohesive frictional ground, Journal of Geotechnical Engineering, ASCE, 119: 675-693.

Livneh, B., and El Naggar, M.H. 2008. Axial testing and numerical modeling of square shaft helical piles under compressive and tensile loading. Canadian Geotechnical Journal, 45(8): 1142–1155.

Meyerhof, G.G., and Adams, J.I. 1968. The ultimate uplift capacity of foundations. Canadian
   Geotechnical Journal, 5(4): 225–244.

Mooney, J.S., Adamczak, S.J., and Clemence, S.P. 1985. Uplift capacity of helix anchors in clay
   and silt. In Proceedings of ASCE Convention, Uplift Behavior of Anchor Foundations in Soil.
   pp. 26–47.

Narasimha Rao, S., Prasad, Y.V.S.N, and Dinakara Shetty, M. 1991. The behavior of model
   screw piles in cohesive soils. Soils and Foundations, 31: 35–50.

Opus Stewart Weir Ltd. 2013. Preliminary geotechnical site investigation: proposed Clover East
   Industrial Park. Sherwood Park, Alta., pp. 46.

Poulos, H. G., and Sim, K. B. 1990. Engineered piles to improve cyclic load capacity, Marine
   Geotechnology, 9:2, 131-140

Randolph, M.F. 2003. Science and empiricism in pile foundation design. Géotechnique, 53 (10):
   847–875.

Randolph, M.F., and Murphy, B.S. 1985. Shaft capacity of driven piles in clay. In Proceedings of
   the 17th Offshore Technology Conference, Houston, Tex., 6–9 May 1985. Offshore
   Technology Conference, Richardson, Tex. Vol. 1, pp. 371–378.

Robertson, P. K., and Cabal Robertson. 2012. Guide to Cone Penetration Testing for
   Geotechnical Engineering, Gregg Drilling & Testing Inc., Signal Hills, Calif.

Rollins, K. M., Olsen, R. J., Egbert, J. J., Jensen, D. H., Olsen, K.G., and Garrett, B.H., 2006,
   Pile Spacing Effects on Lateral Pile Group Behavior: Load Tests. J. Geotech. Geoenviron.
   Eng., 132(10), 1262–1271.

Rybnikov, A.M. 1990. Experimental investigations of bearing capacity of bored-case-in-place
   tapered piles. Soil Mechanics and Foundation Engineering, 27: 48–51.

Salgado, R. 2008. The Engineering of Foundations, McGraw Hill, New York, NY, USA.

Sakr, M. 2015. Relationship between installation torque and axial capacities of helical piles in cohesionless soils, Canadian Geotechnical Journal, 52(6): 747-759.

Seed, H. B., Idriss, I. M., Makdisi, F., and Banerjee, J. 1975. Representation of irregular stress time histories by equivalent uniform stress series in liquefaction analysis. Rep. No. EERC 75-29, Earthquake Engineering Research Center. Univ. of California, Berkeley, Calif.

Skempton AW, Northey RD. 1952. The sensitivity of clays. Géotechnique 3: 30-53

Tappenden, K. M. 2007. Predicting the axial capacity of screw piles installed in Western Canadian soils. M.Sc. thesis, Department of Civil and Environmental Engineering, University of Alberta, Edmonton, Alberta.

Tomlinson, M.J. 1957. The adhesion of piles driven in clay soils. Proceedings, 4th International Conference on Soil Mechanics and Foundation Engineering, London, Vol. 2, pp. 66–71.

Wei, J. and El Naggar, M.H. 1998. Experimental study of axial behavior of tapered piles, Canadian Geotechnical Journal, 35(4): 641-654.

Zhang, D.J. 1999. Predicting capacity of helical screw piles in Alberta soils. MSc thesis, Department of Civil and Environmental Engineering, University of Alberta, AB, Canada.

Appendix A – LoggerNet code for CR3000 datalogger

The code of the instrumented pile load tests

```
'CR3000

'Created by Short Cut (3.1)


'Declare Variables and Units

Public BattV

Public FCLoaded

Public PTemp_C

Public CReps

Public ZMode

Public CIndex

Public CAvg

Public Strain(5)

Public Vr1000(5)

Public BrZero(5)

Public HalfBr(3)

Public LoadCell

Public GFsRaw(5)={2.175,2.175,2.175,2.175,2.175}

Public Mult(3)={150.65,150.68,150.06}

Public Offs(3)={0,0,0}


Alias Strain(1)=StrainST1

Alias Strain(2)=StrainST2

Alias Strain(3)=StrainST3

Alias Strain(4)=StrainST4

Alias Strain(5)=StrainST5
```

Alias HalfBr(1)=LP1

Alias HalfBr(2)=LP2

Alias HalfBr(3)=LP3

Units BattV=Volts

Units PTemp_C=Deg C

Units Vr1000=mV/V

Units BrZero=mV/V

Units LoadCell=kN

Units StrainST1=microstrain

Units StrainST2=microstrain

Units StrainST3=microstrain

Units StrainST4=microstrain

Units StrainST5=microstrain

Units LP1=mm

Units LP2=mV/mV

Units LP3=mV/mV

'Define Data Tables

DataTable(AxlInstr,True,-1)

      DataInterval(0,500,mSec,10)

      Sample(1,LoadCell,FP2)

      Sample(1,LP1,FP2)

      Sample(1,LP2,FP2)

      Sample(1,LP3,FP2)

      Sample(1,StrainST1,IEEE4)

      Sample(1,StrainST2,IEEE4)

      Sample(1,StrainST3,IEEE4)

```
        Sample(1,StrainST4,IEEE4)

        Sample(1,StrainST5,IEEE4)

        Sample(1,Vr1000(1),IEEE4)

        Sample(1,Vr1000(2),IEEE4)

        Sample(1,Vr1000(3),IEEE4)

        Sample(1,Vr1000(4),IEEE4)

        Sample(1,Vr1000(5),IEEE4)

EndTable


DataTable(Table2,True,-1)

        DataInterval(0,1440,Min,10)

        Minimum(1,BattV,FP2,False,False)

EndTable


'Calibration history table

DataTable(CalHist,NewFieldCal,10)

        SampleFieldCal

EndTable


'Main Program

BeginProg

        'Initialize calibration variables for

        'Full Bridge Strain, 350 ohm with 4WFBS350 TIM measurement 'Vr1000()'

        CIndex=1 : CAvg=1 : CReps=5      'Load the most recent calibration values from the CalHist table

        FCLoaded=LoadFieldCal(True)

        'Main Scan

        Scan(500,mSec,1,0)

                'Default Datalogger Battery Voltage measurement 'BattV'
```

Battery(BattV)

'Default Wiring Panel Temperature measurement 'PTemp_C'

PanelTemp(PTemp_C,_60Hz)

'Full Bridge Strain, 350 ohm measurement 'Vr1000()'

BrFull(Vr1000(),5,mV20,1,1,5,1750,True,True,0,250,1,0)

'Calculated strain result 'Strain()' for

'Full Bridge Strain, 350 ohm measurement 'Vr1000()'

StrainCalc(Strain(),5,Vr1000(),BrZero(),6,GFsRaw(),0.3)

'Zeroing calibration for

'Full Bridge Strain, 350 ohm measurement 'Vr1000()'

FieldCalStrain(10,Vr1000(),CReps,0,BrZero(),ZMode,0,CIndex,CAvg,0,Strain())

'Generic Half Bridge measurements 'HalfBr()'

BrHalf(HalfBr(),3,mV5000,17,2,3,5000,True,0,_60Hz,Mult(),Offs())

'Generic Full Bridge measurements 'LoadCell'

BrFull(LoadCell,1,mV20,8,3,1,5000,True,True,0,_60Hz,-211,0)

'Call Data Tables and Store Data

CallTable AxlInstr

CallTable Table2

CallTable CalHist

NextScan

EndProg

The code of the non-instrumented pile load tests

```
'CR3000

'Created by Short Cut (3.1)


'Declare Variables and Units

Public BattV

Public PTemp_C

Public LoadCell

Public HalfBr(3)

Public Mult_2(3)={150.65,150.68,150.06}

Public Offs_2(3)={0,0,0}


Alias HalfBr(1)=LP1

Alias HalfBr(2)=LP2

Alias HalfBr(3)=LP3


Units BattV=Volts

Units PTemp_C=Deg C

Units LoadCell=kN

Units LP1=mm

Units LP2=mV/mV

Units LP3=mV/mV


'Define Data Tables

DataTable(NormTest,True,-1)

        DataInterval(0,500,mSec,10)

        Sample(1,LoadCell,FP2)
```

```
        Sample(1,LP1,FP2)

        Sample(1,LP2,FP2)

        Sample(1,LP3,FP2)

EndTable


DataTable(Table2,True,-1)

        DataInterval(0,1440,Min,10)

        Minimum(1,BattV,FP2,False,False)

EndTable


'Main Program

BeginProg

        'Main Scan

        Scan(500,mSec,1,0)

                'Default Datalogger Battery Voltage measurement 'BattV'

                Battery(BattV)

                'Default Wiring Panel Temperature measurement 'PTemp_C'

                PanelTemp(PTemp_C,_60Hz)

                'Generic Full Bridge measurements 'LoadCell'

                BrFull(LoadCell,1,mV20,8,1,1,5000,True,True,0,_60Hz,-211,0)

                'Generic Half Bridge measurements 'HalfBr()'

                BrHalf(HalfBr(),3,mV5000,17,2,3,5000,True,0,_60Hz,Mult_2(),Offs_2())

                'Call Data Tables and Store Data

                CallTable NormTest

                CallTable Table2

        NextScan

EndProg
```

Appendix B – As-built Structural Design

Reaction System

The reaction system consisted of a reaction beam, two reaction pile groups on the end of the beam. Structural design of the loading frame was based on the estimated capacity of the reaction piles and testing piles. For those piles with length of 1600 mm, the capacity of the piles was directly adapted from a previous LCRA report (LCRA 2012) because those piles have been tested before in similar soil type. For those piles with the length of 3000 mm, the capacity of the piles with same diameters but different lengths were plotted and the corresponding capacity for 3000 mm length was extrapolated by fitting a linear line through the plot. The highest capacity extrapolated was used as the minimum required loading condition in the reaction system, which is 400 kN.

Reaction Piles Design

The preliminary design of the loading frame is a reaction beam supported by two pile groups on the ends. The reaction beam is considered fixed on both ends, and the critical load is applied at one third of the beam length. With the given assumption, calculations were carried out to determine the minimum number and dimension of the reaction pile.

There are a few critical points to be considered. First, according to the LCRA report (LCRA 2012), the pile capacity in cohesionless soil is slightly greater than that in cohesive soil. Secondly, most of the time the compressive capacity of the pile exceeds the tensile capacity of the pile. When the testing pile is under compressive load (push), the reaction piles on the ends of the beam are under tensile load (pull). So the most critical condition that governs the design

would be when the testing pile with the highest capacity is tested under compressive load in cohesionless soil.

The reaction pile group is made of four M114X3000 piles with diameter of 114 mm and length of 3000mm, which is the largest pile available from TerraPro warehouse. While the maximum capacity of the testing pile was estimated to be 400 kN, the maximum tensile load distributed to the reaction pile group would be 267 kN. The tensile capacity of the reaction pile is 162 kN, and so the pile group made up with 4 of the M114X3000 piles led to a factor of safety of 2.4.

However, at the Sherwood Park Site, the highest compressive capacity of the testing piles turned out to be only 145 kN while the estimated value was 262 kN. So it can be concluded that the pile group design was conservative and the factor of safety was higher than 2.4.

Reaction Beam Selection

The objective was to be able to test 2 piles using one loading frame, and the spacing between two testing piles needed to be sufficient to avoid disturbance of the soil. The largest diameter of the piles tested was 114 mm so the spacing needed to be at least 1.2 m. With this constraint, a beam with a length of 3.96 m (13 ft) was selected. Structural analysis was carried out the beam with a length of 3.9 m and both ends fixed. Several failure criterion considered were flexural strength, shear strength, torsional shear strength and maximum deflection. After comparing the minimum size required with the sizes available from the local steel supplier, a W-shape beam with the size W360x179 was selected. The beam was reinforced with two 5/16'' steel plate welded between the flanges along the entire length. The calculation of beam selection can be found in the appendix. Due to the lack of material specification sheet, all calculation was based on the

assumptions are that the material was structural steel with 200 GPa for Young's modulus and 350 MPa for yield strength.

Connections Design

For axial loading tests, the main parts of the loading frame were the reaction beam and the reaction piles. The beam and the piles were connected by the designed connectors and adaptors. Rectangular pile caps were connected to the reaction piles by washer and screws. Each pile cap connected 2 reaction piles, and timber blocks were stacked on top of the pile caps to support the beam. The pile caps were connected to the beam by threaded steel bars and clamps. Each pile came with its original pile cap, but due to lack of information on the material property, a steel pile cap with the same configuration as the original pile cap was screwed on top of the piles to provide more capacity. The hydraulic jack was connected with the load cell by adaptors trough the internal threads, and was kept as one unit throughout the entire project. The top of the load cell was bolted on a rolling unit from the beam in order to save on the installation time between tests, while the bottom of the hydraulic jack was bolted to the testing pile using an adaptor.

References

LCRA. 2012. Engineering report for compression, tension and lateral loading tests on Krinner ground-screw piles. Lymon C. Reese &Associates Inc, Austin, TX.

1.0 Beam Selection

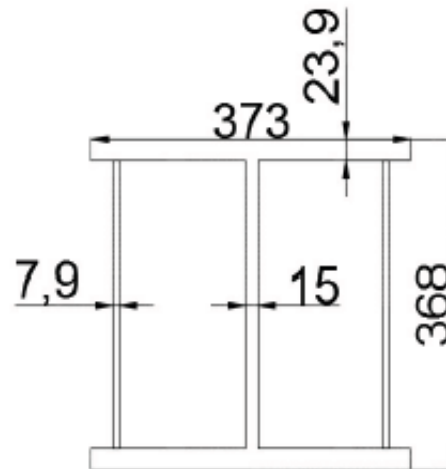### 1.1 Pick W-shape beam W360x179

1.1.1. Define class of a section

$b := 373 \ mm$ $\qquad$ $d := 368 \ mm$

$t := 23.9 \ mm$ $\qquad$ $h := d - 2 \ t = 320.2 \ mm$

$w := 15 \ mm$ $\qquad$ $Fy := 350 \ MPa$

$\dfrac{b}{2 \, t} = 7.803$ $\qquad\qquad$ $\dfrac{b}{2 \, t} < \dfrac{145}{\sqrt{Fy}}$

$\dfrac{145}{\sqrt{350}} = 7.751$

$\dfrac{h}{w} = 21.347$

$\qquad\qquad\qquad\qquad$ $\dfrac{h}{w} < \dfrac{1100}{\sqrt{Fy}}$

$\dfrac{1100}{\sqrt{350}} = 58.797$

This section is a Class 1 section

1.1.2. Flexural Strength.

For Class 1 sections, flexural strength is calculated as following: $\quad Mr = \varphi \cdot Fy \cdot Zx$

$Z_x := 3480 \cdot 10^3 \ mm^3$ $\qquad$ $Fy := 350 \ MPa$ $\qquad$ $M_{max} := 120 \ kN \cdot m$

$t1 := 7.9 \ mm$ $\qquad\qquad$ $\varphi := 0.9$

$Mr := \varphi \cdot Fy \cdot Z_x = \left(1.096 \cdot 10^3\right) \ kN \cdot m$ $\qquad$ $F.S._{bending} := \dfrac{Mr}{M_{max}} = 9.135$

1.1.3. Shear Strength

The shear force is assumed to be carried only by the web of the beam. The shear distribution in the web is assumed to be an uniform distribution. $\qquad Kv = 5.34 \quad constant$

$\qquad\qquad\qquad\qquad\qquad\qquad\qquad\qquad\qquad\qquad$ Will fail in shear yielding

$439 \cdot \sqrt{\dfrac{5.34}{350}} = 54.225$ $\qquad\qquad$ $\dfrac{h}{w} < 439 \cdot \sqrt{\dfrac{Kv}{Fy}}$

$\dfrac{h}{w} = 21.347$

$\varphi := 0.9$ $\quad$ $A_w := d \cdot w = \left(5.52 \cdot 10^3\right) \ mm^2$ $\qquad$ $Fs := \dfrac{Fy}{\sqrt{3}} = 202.073 \ MPa$

$Vr := \varphi \cdot Fs \cdot A_w = 1003.897 \ kN$

$V_{max} := 100 \ kN$

$\qquad\qquad\qquad\qquad\qquad\qquad$ $F.S._{shear} := \dfrac{Vr}{V_{max}} = 10.039$

1.1.4. Deflection

$Ix := 575 \cdot 10^6 \ mm^4$ $\qquad\qquad\qquad\qquad$ $y := 2400 \ mm$ $\qquad$ $P := 150 \ kN$

$$x := 1200 \ mm \qquad l := 3600 \ mm$$

$$E := 200000 \ MPa$$

$$\Delta y_{max} := \frac{P \cdot x \cdot y \cdot (x+2 \ y) \cdot \sqrt{3 \ x \cdot (x+2 \ y)}}{27 \cdot E \cdot Ix \cdot l} = 1.078 \ mm \qquad \text{Less than L/300}$$

1.1.5. Torsion

Assume the load from the testing pile to the reaction beam is offset by 1/4 of the beam width.

$$at := b - 25.4 \ mm \cdot 2 = 322.2 \ mm$$

$$dt := \frac{b}{4} = 93.25 \ mm \qquad th := t1 = 7.9 \ mm \qquad bt := d = 368 \ mm$$
$$th1 := t = 23.9 \ mm$$

$$T := P \cdot dt = 13.988 \ kN \cdot m$$

$$J' := \frac{2 \cdot th \cdot th1 \cdot (at - 2 \ mm)^2 \cdot (bt - th1)^2}{at \cdot th + bt \cdot th1 - th^2 - th1^2} = (4.282 \cdot 10^8) \ mm^4$$

$$L := 1.2 \ m$$
$$G := 77000 \ MPa \qquad \theta := \frac{T \cdot L}{G \cdot J'} = 0.029 \ ^\circ$$

$$\tau a := \frac{T}{2 \cdot t \cdot (at - t) \cdot (bt - t1)} = 2.724 \ MPa \qquad \tau b := \frac{T}{2 \cdot t1 \cdot (at - t) \cdot (bt - t1)} = 8.242 \ MPa$$

Both are way less than Fs=202MPa

1.1.6. Check for lateral-torsional buckling

$$L := 3.6 \ m \qquad\qquad I_y := 207 \cdot 10^6 \ mm^4$$
$$G := 77000 \ MPa \qquad J := 3910 \cdot 10^3 \ mm^4$$
$$E := 200000 \ MPa \qquad C_w := 6120 \cdot 10^9 \ mm^6$$
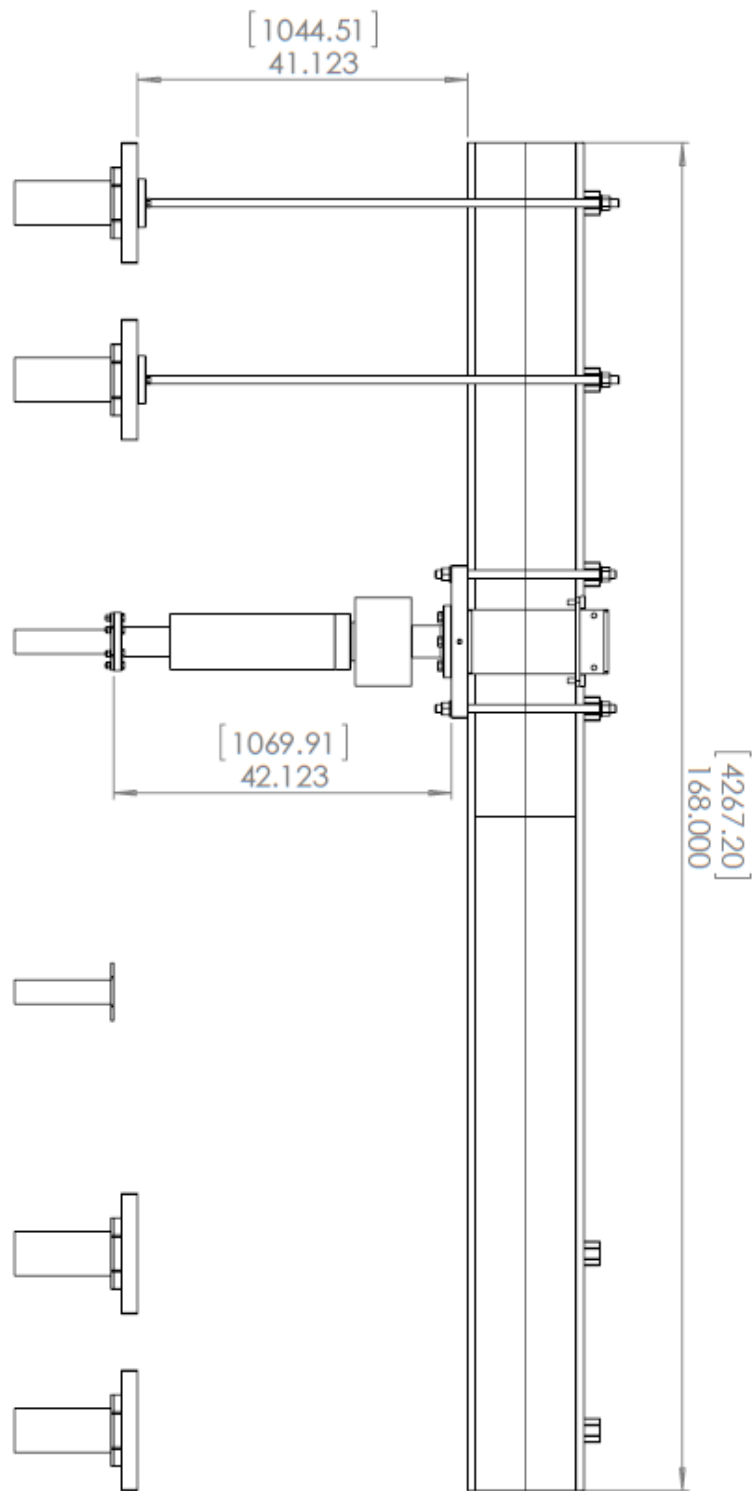
$$M_p := Fy \cdot Z_z = 1218 \ kN \cdot m$$

$$M_u := 1 \cdot \frac{\pi}{L} \cdot \sqrt{E \cdot I_y \cdot G \cdot J + \left(\pi \cdot \frac{E}{L}\right)^2 \cdot I_y \cdot C_w} = 6235.398 \ kN \cdot m$$
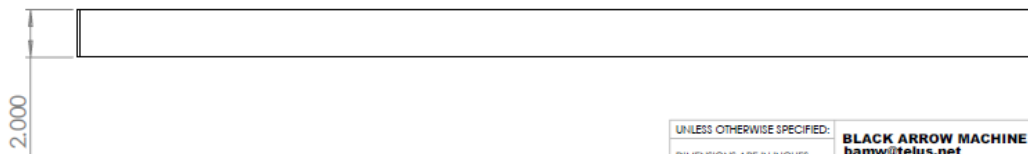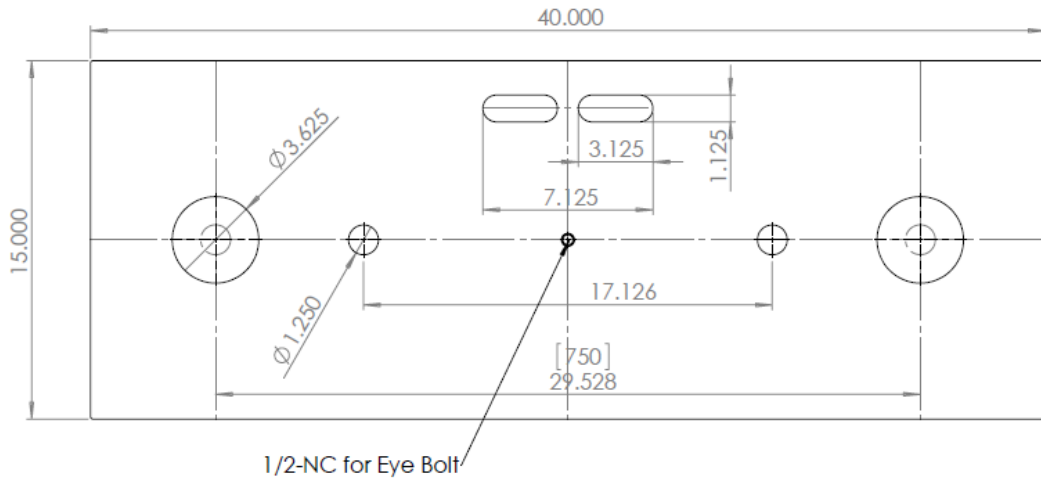
$$M_p \cdot \frac{2}{3} = 812 \ kN \cdot m$$

$$M_u > \frac{2}{3} M_p \qquad M_r := 1.15 \cdot 0.9 \cdot M_p \cdot \left(1 - \frac{0.28 \cdot M_p}{M_u}\right) = 1191.7 \ kN \cdot m$$

Mr is greater than Mr from flexual calculation. lateral-torsional buckling doesn't govern the design.

2.0 Plate Selection

[1044.51]
41.123

[1069.91]
42.123

[4267.20]
168.000

2.1 Plate 1

40.000

15.000

Ø3.625

3.125

1.125

7.125

Ø1.250

17.126

[750]
29.528

1/2-NC for Eye Bolt

2.000

Material 44W
(8) Required

UNLESS OTHERWISE SPECIFIED:	BLACK ARROW MACHINE & WELDING INC. bamw@telus.net 780 489-1156

DIMENSIONS ARE IN INCHES
TOLERANCES:
FRACTIONAL± 0.015
ANGULAR: MACH±   BEND ±
TWO PLACE DECIMAL   ±0.010
THREE PLACE DECIMAL ±0.005

TITLE:
Mounting plates

COMMENTS:

MATERIAL

FINISH

SIZE	DWG. NO.		REV
A	Plates		

DO NOT SCALE DRAWING   SCALE: 1:10 WEIGHT: SHEET 1 OF 5

Treat the pile cap as a simply supported beam
with a width of 15in and a lenghth of 40in.
Reaction force is 25kN, applied load is in the
center of the beam, 50kN.

$Dp := 140 \ mm$ $S := 29.528 \cdot in$ $P := 25 \ kN$ $L := 40 \ in$

$b := 15 \ in$ $M_{max} := P \cdot L = 25.4 \ kN \cdot m$

$I := \dfrac{b \cdot t^3}{12}$ $y := \dfrac{t}{2}$ $\sigma := \dfrac{M_{max} \cdot y}{I}$ $\sigma := 350 \ MPa$

Check for bending moment

$t := 2 \ in$

$300 \ MPa = \dfrac{M_{max} \cdot \dfrac{t}{2}}{\dfrac{b \cdot t^3}{12}}$

$\text{find}(t) = 1.438 \ in$

Check for shear force

$t := 2 \ in$

$\dfrac{300000000}{\sqrt{3}} \ Pa = \dfrac{\dfrac{100 \ kN}{2}}{t\left(\pi \cdot 0.5 \ in\right)}$

$\text{find}(t) = 0.285 \ in$

From above, a conclusion can be made that bending moment criterion governs the
design. The pile cap should have a thickness at least 1.44 in.

Check for F.S
$\sigma := 300 \ MPa$ $b := 15 \cdot in$ $t := 2 \ in$ $I := \dfrac{b \cdot t^3}{12} = \left(4.162 \cdot 10^{-6}\right) m^4$

$y := \dfrac{t}{2} = 0.025 \ m$ $M_{available} := \dfrac{\sigma \cdot I}{y} = 49.161 \ kN \cdot m$ $M_{max} := 12.7 \ kN \cdot m$

$F.S := \dfrac{M_{available}}{M_{max}} = 3.871$

2.2 Plate 3

Determine the minimum size of washer required. Assume the diameter of the washer is 3in.

$\sigma_r := \dfrac{690 \ MPa}{\sqrt{3}} = 398.372 \ MPa$ $F_t := 110 \ kN$

107

1.000

[10.21]
Ø0.402

5/8 NC

[180]
7.087

[198]
7.795
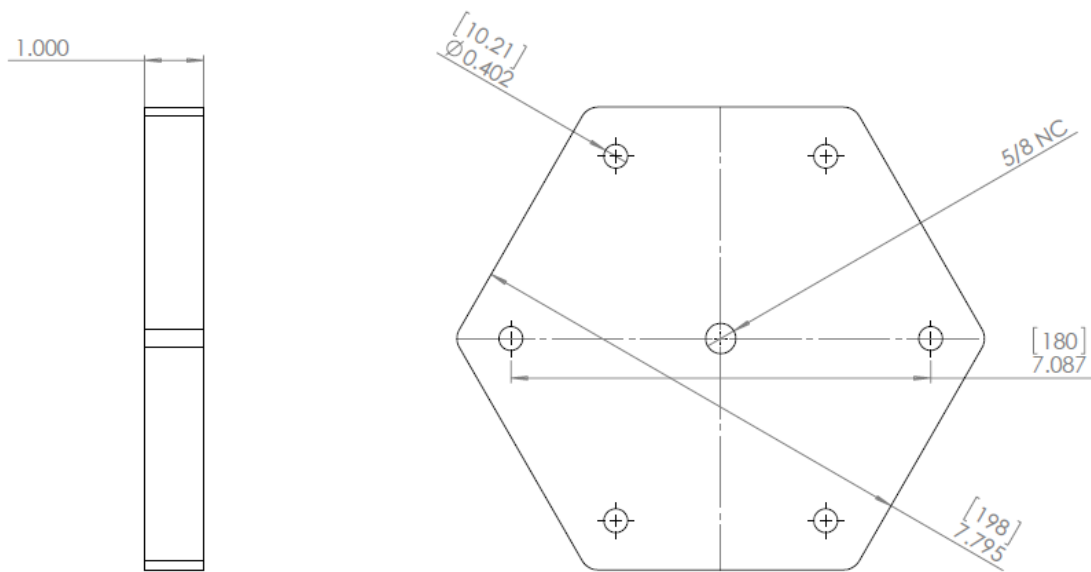
$d := \dfrac{5}{8} \ in$

$t := 1 \ in$

$A_s := \pi \cdot d \cdot t = 1.963 \ in^2$

$\sigma_s := \dfrac{F_t}{A_s} = 86.835 \ MPa$

$F.S. := \dfrac{\sigma_r}{\sigma_s} = 4.588$

Plate 3 is QT-100 Pilling adaptor
plates.

2.3 Clamp Plates

The clamps are 21in long and 3in wide. Assume the clearance between the center of the bar and the edge of the beam is 1.5inch.

Check for F.S (Bending)

$$\sigma := 300 \ MPa \qquad b := 3 \ in \qquad\qquad t := 2 \ in \qquad I := \frac{b \cdot t^3}{12} = \left(8.325 \cdot 10^{-7}\right) \ m^4$$

$$y := \frac{t}{2} = 0.025 \ m \qquad\qquad L := 1.5 \ in \qquad P := \frac{150 \ kN}{4} = 37.5 \ kN$$

$$M_{available} := \frac{\sigma \cdot I}{y} = 9.832 \ kN \cdot m$$

$$M_{max} := P \cdot L = 1.429 \ kN \cdot m$$

$$F.S_{Bending} := \frac{M_{available}}{M_{max}} = 6.882$$

Check for F.S (Shearing)

Assume the diameter of the washer is 1.25in.

$$\sigma := \frac{300}{\sqrt{3}} \ MPa = 173.205 \ MPa$$

$$d := 1.75 \ in \qquad t := 2 \ in$$

$$F_t := 67 \ kN$$

$$A_s := 0.5 \cdot \pi \cdot d \cdot t = 5.498 \ in^2$$

$$\sigma_s := \frac{F_t}{A_s} = 18.889 \ MPa$$

$$F.S. := \frac{\sigma}{\sigma_s} = 9.169$$